arXiv:cond-mat/0201407v2 [cond-mat.str-el] 15 Apr 2002

Electronic Structure and Phase Transition in V_2O_3: Importance of 3d Spin-Orbit Interaction and Lattice Distortion

Arata Tanaka

Department of Quantum Matter, ADSM
Hiroshima University, Higashi-Hiroshima 739-8530, Japan

(Received)

The 3d electronic structure and phase transition in pure and Cr doped V_2O_3 are theoretically investigated in relation to the 3d spin-orbit interaction and lattice distortion. A model consisting of the nearest-neighbor V ion pair with full degeneracy of the 3d orbitals is studied within the many-body point of view. It is shown that each V ion with $S = 1$ spin state has a large orbital magnetic moment $\sim 0.7\mu_B$ and no orbital ordering occurs in the antiferromagnetic insulating (AFI) phase. The anomalous resonant Bragg reflection found in the AFI phase is attributed to the magnetic ordering. In the AFI and paramagnetic insulating (PI) phases, Jahn-Teller like lattice instability leads to tilting of the V ion pairs from the corundum c-axis and this causes large difference in the orbital occupation between the paramagnetic metal and the insulating phases, which is consistent with linear dichroic V 2p XAS measurements. To understand the AFI to PI transition, a model spin Hamiltonian is also proposed. The transition is found to be simultaneous order-disorder transition of the magnetic moments and tilting directions of the V ion pairs. Softening of elastic constant C_{44} and abrupt change in short range spin correlations observed at the transition are also explained.

KEYWORDS: V_2O_3, electronic structure, phase transition, lattice distortion, orbital ordering, spin-orbit interaction, orbital moment, resonant x-ray scattering, V 2p XAS

§1. Introduction

The metal-insulator (Mott) transition in V_2O_3 have been extensively studied ever since Mott suggested the possibility of the localization of electrons driven by Coulomb repulsion.1) Above the transition temperature $T_N \sim$ 155K, the material is paramagnetic metal (PM) and has the corundum structure with the trigonal symmetry (space group $R\bar{3}c$). Below T_N, it is an antiferromagnetic insulator (AFI) and the lattice distortion to the monoclinic structure ($I2/a$) takes place.2) Cr doped alloys $(V_{1-x}Cr_x)_2O_3$ exhibit also interesting features.3, 4, 5, 6, 7) For $0.005 < x < 0.018$, at a temperature above the AFI → PM transition, the material further undergoes a PM to paramagnetic insulator (PI) phase transition with no change in the crystal structure. For much higher Cr concentration $x > 0.018$, the PM phase disappears and a AFI → PI transition takes place.

Although V_2O_3 and its alloys are often referred to a typical example of the Mott-Hubbard system, there are experimental facts showing the complex aspects of these materials, which can not be explained by the simple single-band Hubbard model. In the AFI phase, they exhibit unusual magnetic order, which breaks corundum trigonal symmetry.8) Neutron scattering experiments have been performed by Bao *et al.* and abrupt change in spatial spin correlation functions has been reported both at the AFI → PM and the AFI → PI transitions.9, 10) This switching of spin correlation indicates that the phase transitions can not be considered as usual order-disorder magnetic transition. Softening of the C_{44} elastic constant has been observed in ultrasonic wave11) and neutron scattering12) experiments at the AFI → PI transition, indicating nearly second order feature of this phase transition as well as strong electron-lattice coupling.

Even now, the electronic structure of these materials are still controversial problem and above experimental facts suggest that much realistic model including the orbital degeneracy of the 3d orbital and the lattice distortion is necessary to explain them. In V_2O_3, the O_h crystal field splits the 3d orbitals of each V ion into two fold e_g and three fold t_{2g} orbitals and the t_{2g} orbitals are further separated into low laying two fold e^π and non-degenerate a_1 orbitals by small trigonal field. In localization limit, two 3d electrons in the V^{3+} ion are accommodated in the lowest e^π orbitals with $S = 1$ spin state. Castellani *et al.* have proposed a model including these e^π and a_1 orbitals.13) In the corundum structure, two V ions forms pairs along the c-axis and in their model, the a_1 orbitals on two V ions of the pair forms molecular orbitals. The bonding a_1 orbital accommodates two electrons out of four in the pair and remaining two electrons occupies one of e^π orbital in each V ions, resulting in $e^\pi a_1$ configuration with $S = 1/2$ spin state in each V ion. They also propose a long-range ordering of orbital occupation in the two fold e^π orbital to explain the complex antiferromagnetic ordering in the AFI phase.

However, recent measurements on the linear dichroism of V 2p x-ray absorption spectra (XAS) in V_2O_3 have revealed that the 3d electron configuration is not $S = 1/2$ $e^\pi a_1$ but mixture of $e^\pi e^\pi$ and $e^\pi a_1$ with $S = 1$ Hund's rule spin state.14) In addition, large differences in $e^\pi e^\pi$ to $e^\pi a_1$ ratio have been found among the AFI, PI and PM phases. Indeed, such $S = 1$ Hund's rule spin state is also obtained in recent "LDA+U"[15,16] band structure calculation,[17] in which a $S = 1$ $e^\pi e^\pi$ ground state having experimentally observed antiferromagnetic order with no orbital degeneracy is favorable for the low temperature monoclinic phase. Mila *et al.* have proposed a model with a large intraatomic exchange interaction.[18,19] In this model, spin state in each V ion remains being $S = 1$ even with strong hybridization between a_1 orbitals. The electronic state of the V ion pair is described as a superposition of two configurations with equal weight: $e^\pi a_1; e^\pi e^\pi$ (the $e^\pi a_1$ configuration in one of V ion and the $e^\pi e^\pi$ configuration in the other) and $e^\pi e^\pi; e^\pi a_1$. In this model, two fold orbital degeneracy is present in this V_2 molecular orbital and the complex antiferromagnetic order in the AFI phase is stabilized with a ferro-type order of this V_2 molecular orbital.

Paolasini *et al.* have performed resonant x-ray scattering experiments (RXS) at the V K-edge on V_2O_3 and they insisted that resonant Bragg peaks observed in the AFI phase are due to the $3d$ orbital ordering.[20,21] However, Lovesey and Knight have argued that the resonant Bragg peaks arise from the ordered orbital magnetic moments of the V ions.[23] Indeed, nonresonant magnetic scattering has been also measured and a large contribution from the orbital magnetic moment to the total magnetic moment $M_L/M_S \sim -0.3$ was found.[20] It is thus important to know how the $3d$ spin-orbit interaction affects the $3d$ electronic structure of V_2O_3. Since this interaction couples spin and orbital degrees of freedom, in the presence of a large orbital angular momentum, no orbital ordering is expected in the AFI phase. In above mentioned theories on the electronic structure of V_2O_3, however, the effects of the $3d$ spin-orbit interaction in the V ions is presumed to be small.

The purpose of this paper is to clarify the effects of the $3d$ spin-orbit interaction and the lattice distortion on the $3d$ electronic structure and the phase transitions of the pure and Cr doped V_2O_3. To this end, first of all, a V ion pair model similar to that proposed by Mila *et al.* will be considered taking into account the $3d$ spin-orbit interaction in § 2. With the $3d$ spin-orbit interaction, no orbital ordering is expected in the AFI phase and instead of this, a large orbital magnetic moment $\sim 0.7\mu_{\rm B}$ is induced in the ground state. The relation between the monoclinic distortion and the magnetic anisotropy and difference in the configuration of the $3d$ electrons between the AFI and PM phases will be also discussed. Second, interaction between the electronic state of the V ion pair and local lattice distortion caused by displacement of the pair will be discussed in § 3. It will be shown that Jahn-Teller like lattice instability occurs when the energies of the $e^\pi a_1; e^\pi e^\pi$ ($e^\pi e^\pi; e^\pi a_1$) and $e^\pi e^\pi; e^\pi e^\pi$ states are nearly degenerate. Third, relation between the magnetic ordering and the lattice distortion in the AFI phase and also the mechanism of the AFI → PI transition will be discussed in § 4. For this purpose, an effective Hamiltonian with exchange interaction between the V ion pairs including lattice distortion effects is proposed. Softening of the elastic constant C_{44} and abrupt change in short range spin correlation functions observed at the AFI → PI transition are reproduced with the model. Finally, to confirm the validity of the present model, recent experiments on RXS and the linear dichroic V $2p$ XAS spectra are analyzed in § 5 and § 6, respectively. The experimental results are well explained within the present model.

§2. V ion Pair Model

2.1 Model Hamiltonian

Each V ion in the corundum structure of V_2O_3 is octahedrally surrounded by six oxygen ions (see Fig. 1). An octahedral crystal field and hybridization between the V $3d$ and O $2p$ orbitals split the energy level of the $3d$ orbital into the e_g and t_{2g} levels and the low laying t_{2g} orbitals accommodate two electrons in each V^{3+} ion. A small trigonal distortion of the oxygen octahedron along the $\boldsymbol{c}_h$-axis further splits the t_{2g} level into a doubly degenerate e^π and a non-degenerate a_1 levels with the C_{3v} symmetry. In the corundum structure, the layers of the honeycomb lattice of V ions are stacking along the $\boldsymbol{c}_h$-axis and each V ion in the layers forms a V ion pair along the $\boldsymbol{c}_h$-axis with a V ion in the adjacent layer. While the a_1 orbitals point to the direction of the $\boldsymbol{c}_h$-axis, forming strong σ bonds in the V ion pairs, the e^π orbitals extend their lobes toward the direction perpendicular to the $\boldsymbol{c}_h$-axis, having π bonds with the three neighbors in the layer.

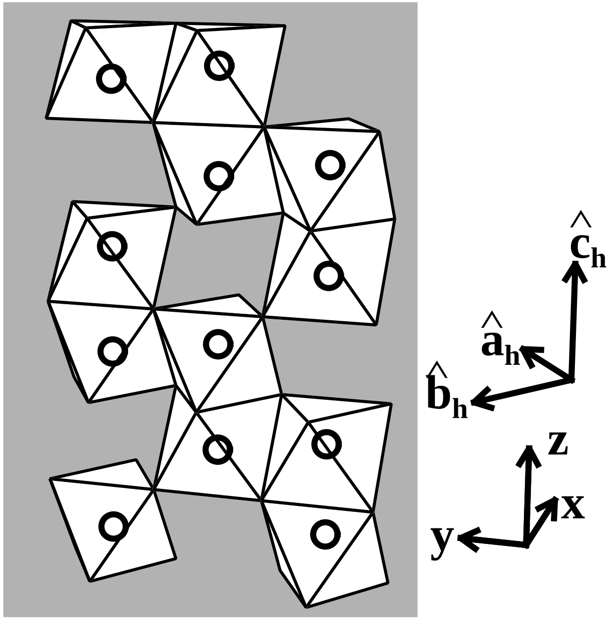

Fig. 1. Corundum structure of V_2O_3. Each V ion (open circles) is octahedrally surrounded by six oxygen ions (octahedra). Along the $\boldsymbol{c}_h$-axis, the V ion pairs surrounded by the face-sharing two oxygen-octahedra are seen whereas in $\boldsymbol{a}_h$-$\boldsymbol{b}_h$ plane, each V ion has three neighbors with edge-sharing oxygen-octahedra.

As was first suggested by Allen, here, it is assumed that the electrons are delocalized within the nearest-neighbor V ion pair and interaction between much father V ions is week.[22] The two V ions of the pair along the $\boldsymbol{c}_h$-axis and electron hopping between them were considered based on configuration interaction approach.[24,25,26] In each V ion site, the fivefold $3d$ orbitals are fully included and the Coulomb and exchange interactions among $3d$ electrons, the $3d$ spin-orbit interaction and the trigonal crystal field are considered.[27)] The Hamiltonian for the V ion pair model then would be written as

$$
\begin{aligned}
H_{\mathrm{elec}} &= \sum_{i,\nu} \varepsilon_d(\nu) n_{i\nu} + \frac{U_{dd}}{2} \sum_{i,\nu,\nu'} n_{i\nu} n_{i\nu'} \\
&+ \sum_{\nu,\nu'} V(\nu,\nu')(a^\dagger_{A,\nu} a_{B,\nu'} + a^\dagger_{B,\nu} a_{A,\nu'}) \\
&+ \sum_{i,\nu_1,\ldots,\nu_4} g(\nu_1,\nu_2;\nu_3,\nu_4) a^\dagger_{i\nu_1} a^\dagger_{i\nu_2} a_{i\nu_4} a_{i\nu_3} \\
&+ \zeta_d \sum_{i,\nu,\nu'} \langle \nu | \boldsymbol{l} \cdot \boldsymbol{s} | \nu' \rangle a^\dagger_{i\nu} a_{i\nu'} \\
&+ \sum_{i,\nu \neq \nu'} C_i(\nu,\nu') a^\dagger_{i,\nu} a_{i,\nu'}, \qquad (1)
\end{aligned}
$$

where the first and second terms are those for the one body energies of the $3d$ orbitals, the effective Coulomb repulsion energy between the $3d$ electrons, respectively, the third term represents the electron hopping between two V ion sites A and B in the V ion pair given in terms of the Slater-Koster parameters $dd\sigma$ and $dd\pi$, the forth term is for the multipole interaction between the $3d$ electrons, which is described by the Slater integrals F^2_{dd} and F^4_{dd} of the $3d$ orbital and the fifth term denotes the $3d$ spin-orbit interaction with the coupling constant ζ_d. The last term represents crystal field due to the monoclinic lattice distortion in the AFI phase. Here, ν represents the combined index of the species of the $3d$ orbital and the spin quantum number of the electron, $i = A, B$ stands for the V ion site and $a^\dagger_{i\nu}$ creates an electron on the $3d$ orbital with ν at the V ion site i.

In a C_{3v} crystal field, the five degenerate $3d$ orbitals split into one non-degenerate a_1 orbital and two doubly-degenerate e orbitals. Using coordinates where z-axis is parallel to the $\boldsymbol{c}_h$-axis of the corundum structure and y-axis to one of the three V-V bond direction in the $\boldsymbol{a}_h$-$\boldsymbol{b}_h$ basal plane (see Fig. 1), the wavefunctions for the $3d$ orbitals in terms of the C_{3v} basis functions are written as

$$
\begin{aligned}
|a_1 : i\rangle &= |3z^2 - r^2\rangle, \\
|e^\pi_u : i\rangle &= s_i \sqrt{\frac{2}{3}} |x^2 - y^2\rangle - \sqrt{\frac{1}{3}} |zx\rangle, \\
|e^\pi_v : i\rangle &= -s_i \sqrt{\frac{2}{3}} |xy\rangle - \sqrt{\frac{1}{3}} |yz\rangle, \\
|e^\sigma_u : i\rangle &= s_i \sqrt{\frac{1}{3}} |x^2 - y^2\rangle + \sqrt{\frac{2}{3}} |zx\rangle, \\
|e^\sigma_v : i\rangle &= -s_i \sqrt{\frac{1}{3}} |xy\rangle + \sqrt{\frac{2}{3}} |yz\rangle,
\end{aligned}
$$

where the two kinds of e orbitals in the C_{3v} symmetry originating from the t_{2g} (e_g) orbitals in the O_h symmetry is specified by superscript π (σ), the subscripts u and v indicate two different kinds of basis functions in each e symmetry orbitals and s_i takes either $+1$ or -1 depending on the orientation of the oxygen octahedron surrounding the i-th V ion site and has different sign between the two V ions in each V ion pair. The energies of these orbitals $\varepsilon_d(\nu)$ can be expressed in terms of the octahedral Dq and the trigonal D_{trg} crystal fields parameters:

$$
\begin{aligned}
\varepsilon_d(a_1) &= -4Dq + 2D_{\mathrm{trg}}/3, \\
\varepsilon_d(e^\pi_u) &= \varepsilon_d(e^\pi_v) = -4Dq - D_{\mathrm{trg}}/3, \\
\varepsilon_d(e^\sigma_u) &= \varepsilon_d(e^\sigma_v) = 6Dq.
\end{aligned}
$$

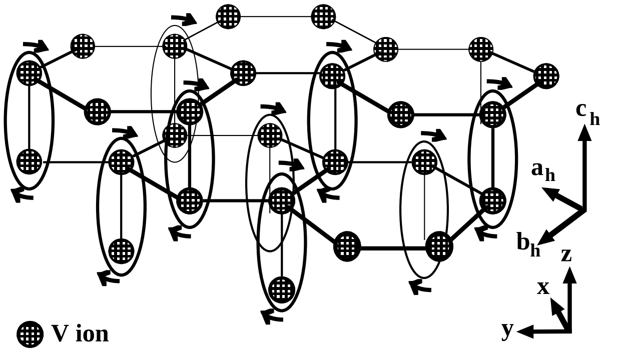

Fig. 2. Schematic drawing of the monoclinic distortion of V_2O_3 in the AFI phase. The circles denote V ions and the ovals show the V ion pairs. The allows represent the directions of the tilting of the V ion pairs in the AFI phase.

In the AFI phase, the crystal structure is distorted from the corundum structure to the monoclinic one. This distortion causes tilting of the V-V bond direction of every V ion pair from the z-axis toward the negative side of the y-axis and breaks three fold rotational symmetry (see Fig. 2). A low symmetry crystal field, which hybridizes the e_v and a_1 orbitals and also the e_v and e_u orbitals on the same site, is present in this phase. Although there are five independent parameters for this low symmetry crystal field $C_i(e^\pi_v, a_1)$, $C_i(e^\pi_u, e^\pi_v)$, $C_i(e^\sigma_v, a_1)$, $C_i(e^\sigma_v, e^\sigma_u)$ and $C_i(e^\pi_v, e^\sigma_u)$, the most important are those related to the e^π orbitals: $C_i(e^\pi_v, a_1)$ and $C_i(e^\pi_u, e^\pi_v)$. Other three parameters involving e^σ orbitals are, for simplicity, all assumed to be zero. Note that there are relations between these parameters for the two V ion sites in the pair: $C_{\mathrm{A}}(e^\pi_v, a_1) = C_{\mathrm{B}}(e^\pi_v, a_1)$, $C_{\mathrm{A}}(e^\pi_u, e^\pi_v) = -C_{\mathrm{B}}(e^\pi_u, e^\pi_v)$.

From recent analysis of high-energy spectroscopy spectra, V_2O_3 is not simply ascribed to the Mott-Hubbard type insulator, where the $3d$ orbital is the main component of the valence-band top and the conduction-band bottom, but intermediate between the Mott-Hubbard and charge-transfer type insulators, where both the valence-band top and conduction-band bottom consist of highly mixed states of the $3d$ and O $2p$ orbitals.[28, 29, 30)] It should be emphasized that although the model we assume here does not contain the O $2p$ orbitals explicitly, the effects of the hybridization between the $3d$ and $2p$ orbitals can be partially included by using renormalized parameters. As will be discussed next section, the on-site effective Coulomb energy between the $3d$ electrons should be strongly renormalized by this d-p hybridization.

2.2 *Effect of d-p hybridization*

Before discussing the details of the ground state properties obtained from the model, in this subsection, we will briefly consider the effects of hybridization between the V $3d$ and the nearest neighbor O $2p$ orbitals. To this end, here we compare a single V^{3+} ion model with a VO_6 cluster model,[24)] in which the V $3d$ orbital and $2p$ orbitals of the six oxygens surrounding the V ion octahedrally are included. The parameters adopted in the cluster model are the effective on-site $3d$-$3d$ Coulomb energy U_{dd}=4.0 eV, the charge transfer energy between the $3d$ and $2p$ orbitals $\Delta = 4.0$ eV, the Slater-Koster parameters for the $3d$-$2p$ hybridization $pd\sigma = -1.73$ eV and $pd\pi = 0.75$ eV and the octahedral crystal field $10Dq = 1.0$ eV. These parameter values are deduced from the high-energy spectroscopy experiments.[28)] The configurations $3d^{2+n}\underline{L}^n$ $(n = 0, 1, 2, 3)$ are assumed for the ${VO_6}^{9-}$ cluster, where $\underline{L}$ denotes a hole in the O $2p$ orbital. For the Slater integrals of the $3d$-$3d$ multipole interactions F^2_{dd} and F^4_{dd}, the atomic Hartree-Fock values reduced to 80% are used for the VO_6 cluster model.

Table I. Eigen energies relative to the ground state energy for the lowest ten states calculated with the VO_6^{9-} cluster and the V^{3+} ion models are shown. The representation in the O_h symmetry and dominant electron occupation in the $3d^2$ configuration of each eigen state (enclosed by the parentheses) are also listed.

Eigen state		Energy (eV) Cluster	Ion
$^3T_1$	(t^2_{2g})	0	0
$^1T_2$	(t^2_{2g})	1.40	1.37
^1E	(t^2_{2g})	1.42	1.40
$^3T_2$	$(t_{2g}e_g)$	1.70	1.53
$^3T_1$	$(t_{2g}e_g)$	2.68	2.82
$^1A_1$	(t^2_{2g})	2.81	2.84
$^1T_2$	$(t_{2g}e_g)$	3.14	3.10
$^1T_1$	$(t_{2g}e_g)$	3.39	3.23
$^3A_2$	(e^2_g)	3.57	3.42
^1E	(e^2_g)	4.86	4.77

In Table I, the lowest ten eigen energies with respect to the ground state energy calculated with the ${VO_6}^{9-}$ cluster and the single V^{3+} ion models are listed. For simplicity, the $3d$ spin-orbit interaction is not considered in both the models. For the V^{3+} ion model, the Slater integrals $\tilde{F}^{2,4}_{dd}$ reduced to 90% of those for the cluster model and $10\tilde{D}q = 1.7$ eV are adopted for the V^{3+} ion model. In the ground state of the ${VO_6}^{9-}$ cluster model, the weights of the configurations $3d^2$, $3d^3\underline{L}$, $3d^4\underline{L}^2$ and $3d^5\underline{L}^3$ are 41.8%, 44.6%, 12.5% and 1.1%, respectively. Although such strong $3d$-$2p$ hybridization, it is clearly seen in Table I that the energy level scheme of the ${VO_6}^{9-}$ cluster is well reproduced by the V^{3+} ion model with the renormalized parameters $\tilde{F}^{2,4}_{dd}$ and $10\tilde{D}q$. Similar low laying level correspondence was found between the ${VO_6}^{10-}$ cluster and V^{2+} $(3d^1)$ ion calculations and also between the ${VO_6}^{8-}$ cluster and V^{4+} $(3d^3)$ ion calculations. Because of this correspondence of the energy levels of the two, the V ion model would be good starting point to describe the electronic state of V_2O_3.

The effective on-site Coulomb energy between "$3d$ electrons" for the V ion model is greatly reduced compared to the model with the O $2p$ orbitals. The on-site effective Coulomb energy between two different "t_{2g} orbitals" $\tilde{U}'$ can be estimated from the VO_6 cluster model by $\tilde{U}' = E_g({VO_6}^{8-}) + E_g({VO_6}^{10-}) - 2E_g({VO_6}^{9-})$, where E_g's denote the ground state energies of the clusters with different charges. The on-site Coulomb energy between electrons on the same "t_{2g} orbital" $\tilde{U}$ and the on-site exchange energy of the "t_{2g} orbitals" $\tilde{J}$ was obtained by using $\tilde{U} = \tilde{U}' + 6\tilde{F}_2 + 40\tilde{F}_4$ and $\tilde{J} = 3\tilde{F}_2 + 20\tilde{F}_4$.[27)] The values obtained are $\tilde{U} = 3.61$ eV, $\tilde{U}' = 2.31$ eV and $\tilde{J} = 0.65$ eV. Similarly, the renormalized value for U_{dd} was obtained by $\tilde{U}_{dd} = \tilde{U}' + \frac{4}{9}\tilde{F}_2 - 10\tilde{F}_4 = 2.07$ eV. These are the values which should be used in models in which the O $2p$ orbitals are not explicitly included. For comparison, these quantities for the bare t_{2g} orbitals obtained with $U_{dd} = 4.0$ eV and $F_{2,4}$ reduced to 80% from Hartree-Fock values are $U = 5.60$ eV, $U' = 4.15$ eV and $J = 0.73$ eV.

Table II. Values of the renormalized parameters adopted in the V ion pair model. For the d-d hopping integrals and the crystal field parameters $C_A(e^\pi_v, a_1)$ and $C_A(e^\pi_u, e^\pi_v)$, values for the AFI and PM phases are indicated. All values are units of eV.

			(AFI)	(PM)
U_{dd}	2.07	$dd\sigma$	−0.735	−0.793
F^2_{dd}	7.29	$dd\pi$	0.100	0.109
F^4_{dd}	4.57	$dd\delta$	0	0
$10Dq$	1.7	$C_A(e^\pi_v, a_1)$	0.02	0
ζ_d	0.023	$C_A(e^\pi_u, e^\pi_v)$	−0.02	0

Because of this strong d-p mixing, the hopping integrals $dd\sigma$, $dd\pi$ and $dd\delta$ between the two V ion sites in the pair must be also renormalized. Effective d-d hopping matrix elements, where the influence of the d-p mixing is considered within the second-order perturbation theory, are

$$V(a_1, a_1) \simeq \frac{1}{N_\pi}\Big(dd\sigma - \frac{2(pd\pi)^2}{3\Delta}\Big),$$

$$V(e^\pi_\gamma, e^\pi_\gamma) \simeq \frac{1}{N_\pi}\Big(-\frac{1}{3}dd\pi + \frac{2}{3}dd\delta + \frac{4(pd\pi)^2}{3\Delta}\Big),$$

$$V(e^\sigma_\gamma, e^\sigma_\gamma) \simeq \frac{1}{N_\sigma}\Big(-\frac{2}{3}dd\pi + \frac{1}{3}dd\delta + \frac{(pd\sigma)^2}{2\Delta}\Big),$$

$$V(e^\sigma_\gamma, e^\pi_\gamma) = V(e^\pi_\gamma, e^\sigma_\gamma) \simeq \frac{\sqrt{2}}{3\sqrt{N_\pi N_\sigma}}\Big(dd\pi + dd\delta - \frac{\sqrt{6}(pd\pi)(pd\sigma)}{\Delta}\Big),$$

where $\gamma = u, v$, $N_\pi = 1 + 4(pd\pi)^2/\Delta$ and $N_\sigma = 1 + 6(pd\sigma)^2/\Delta$. Using parameter values for $pd\sigma$, $pd\pi$ and Δ deduced from the high-energy spectroscopy experiments mentioned before, it is found that values of the matrices other than $V(a_1, a_1)$ is largely reduced from those without d-p hybridization. Such the effects of the d-p hybridization was included approximately by reducing the value of $dd\pi$ to 25% from the bare value. Harrison's values are adopted as for the bare values of the d-d hopping integrals.[31] The renormalized parameters adopted in the V ion pair model are summarized in Table. II.

2.3 Properties of ground state

In this subsection, we will discuss the ground state properties of the V_2O_3, using the model described in § 2.1. In Fig. 3(a), the trigonal crystal field D_{trg} dependence of the a_1 orbital occupation number for a V ion in the ground state for the PM phase is shown. Two discontinuous decrease in the occupation number at $D_{\mathrm{trg}} = 0.09$ eV and $D_{\mathrm{trg}} = 0.34$ eV are seen as D_{trg} increases. Because of the Hund's rule coupling, the spins of two electrons in each V ion site form $S = 1$ spin state in the ground state. This is very different result to the model proposed by Castellani *et al.*,[13] where one electron-spin in the a_1 orbital couples to that of the other V ion of the pair forming a singlet spin state with the neighboring site and $S = 1/2$ spin degree of freedom arising from the other electron in the the e^π orbital remains in each V ion site. The difference in the spin state of the V ions is essentially caused by their choice of the on-site exchange interaction value $\tilde{J} \sim 0.2$ eV, which is less than one third of our value. For $D_{\mathrm{trg}} < 0.09$ eV, where energy of the a_1 orbital is lower than that of the e^π orbital, one of electrons is in the e^π orbital and the other is in the a_1 orbital in both V ion sites (denoted by $e^\pi a_1; e^\pi a_1$). On the other hand, for $D_{\mathrm{trg}} > 0.34$ eV, two e^π orbital are occupied in both V ion site (denoted by $e^\pi e^\pi; e^\pi e^\pi$). In between these two region, the ground state is a superposition of the $e^\pi e^\pi; e^\pi a_1$ and $e^\pi a_1; e^\pi e^\pi$ states.

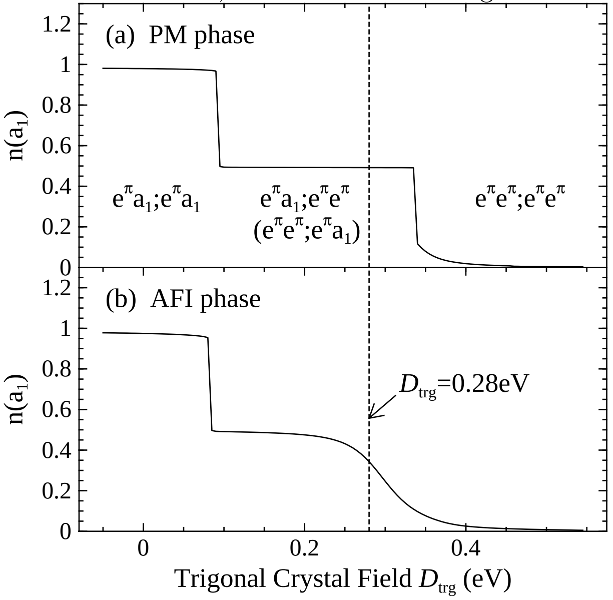

Fig. 3. Trigonal crystal field D_{trg} dependence of the a_1 orbital occupation number per V ion in the ground state for the PM (a) and AFI (b) phases are shown. The vertical line is positioned at $D_{\mathrm{trg}} = 0.28$ eV where the ground state gives the ratio $e^\pi a_1 : e^\pi e^\pi = 1 : 2$ deduced from the XAS experiment for the AFI phase.

For $0.09 < D_{\mathrm{trg}} < 0.34$, the ground state is doublet state and their wave functions $|g\pm\rangle$ in large U and $10Dq$ limit can be approximately described by

$$|g+\rangle = \frac{1}{\sqrt{2}}(|e^\pi_{+\uparrow} a_{1\uparrow}; e^\pi_{+\uparrow} e^\pi_{-\uparrow}\rangle + |e^\pi_{+\uparrow} e^\pi_{-\uparrow}; e^\pi_{+\uparrow} a_{1\uparrow}\rangle),$$
$$|g-\rangle = \frac{-1}{\sqrt{2}}(|e^\pi_{-\downarrow} a_{1\downarrow}; e^\pi_{+\downarrow} e^\pi_{-\downarrow}\rangle + |e^\pi_{+\downarrow} e^\pi_{-\downarrow}; e^\pi_{-\downarrow} a_{1\downarrow}\rangle),$$

where ↑ (↓) denotes the magnetic quantum number of the electron spin $s_z = 1/2$ ($s_z = -1/2$) and $|e^\pi_\pm\rangle = \frac{1}{\sqrt{2}}(\mp|e^\pi_u\rangle - \mathrm{i}|e^\pi_v\rangle)$ with $\langle e^\pi_\pm|L_z|e^\pi_\pm\rangle = \mp 1$. These states have the orbital and spin angular momenta along the z-axis and the values per V ion are $\langle g\pm|L_z|g\pm\rangle = \mp\frac{1}{2}$ and $\langle g\pm|S_z|g\pm\rangle = \pm 1$. Since this degeneracy of ground state is magnetic, there is no orbital degree of freedom. This is very different result to the similar V ion pair model propose by Mila *et al.*,[18, 19] where the orbital angular momentum is assumed to be small and thus the orbital degree of freedom still remains apart from the spin degree of freedom. The ground state wave functions of their model are written as

$$|g\gamma; S^{\mathrm{T}}_z\rangle = \frac{1}{\sqrt{2}}(|e^\pi_\gamma a_1; e_u e^\pi_v\rangle + |e^\pi_u e^\pi_v; e^\pi_\gamma a_1\rangle) \otimes |S^{\mathrm{T}} = 2; S^{\mathrm{T}}_z\rangle,$$

where γ specifies the two kinds of the e^π orbitals u and v and $|S^{\mathrm{T}} = 2; S^{\mathrm{T}}_z\rangle$ is the total-spin wavefunction, in which $S = 1$ Hund's spins of the two V ions are coupled ferromagnetically. The ground state wavefunctions of our model $|g\pm\rangle$ can be describe in terms of the wavefunctions $|g\gamma; S^{\mathrm{T}}_z\rangle$ as

$$|g\pm\rangle = \frac{1}{\sqrt{2}}(-\mathrm{i}|gu; S^{\mathrm{T}}_z = \pm 2\rangle \pm |gv; S^{\mathrm{T}}_z = \pm 2\rangle). \qquad (2)$$

The wavefunctions of Mila's ground state other than above two are lifted higher energies ranging up to ~ 0.027 eV.

It has been reported from the x-ray diffraction experiment that the distortion from the corundum structure to the monoclinic structure at the PM → AFI transition involves abrupt expansion of the V-V bond length of the V ion pair and rotation of the V-V bond direction about 1.8° from the $\boldsymbol{c}_h$-axis (within the y-z plane in Fig. 2).[2] To take into account the effects of the lattice distortion, the values of $dd\sigma$ and $dd\pi$ are reduced from those for the PM phase using the V-V distance R dependence $(ddm) \propto 1/R^5$ proposed by Harrison[31] and the low symmetry crystal field are considered as in Table II.

In Fig. 3(b), the trigonal field D_{trg} dependence of the a_1 orbital occupation number in the ground state for the AFI phase is shown. The most different part compared to Fig. 3(a) is that the occupation number decreases continuously as D_{trg} increases around $D_{\mathrm{trg}} \sim 0.3$ eV. This indicates that the boundary between the $e^\pi e^\pi; e^\pi e^\pi$ and $e^\pi a_1; e^\pi e^\pi$ ($e^\pi e^\pi; e^\pi a_1$) states is obscure and around $D_{\mathrm{trg}} \sim 0.3$ eV, there is $e^\pi e^\pi; e^\pi e^\pi$ and $e^\pi a_1; e^\pi e^\pi$ ($e^\pi e^\pi; e^\pi a_1$) mixed state. This can be understood as follows. Because of the symmetry lowering of the pair caused by the tilting of the V-V bond direction from the trigonal axis, the a_1 and e^π_v orbitals hybridized in each other. This leads to hybridization of the $e^\pi e^\pi; e^\pi e^\pi$ and $e^\pi a_1; e^\pi e^\pi$ ($e^\pi e^\pi; e^\pi a_1$) states around $D_{\mathrm{trg}} \sim 0.3$ eV, where energies of these two states are almost degenerate. It is also seen in Fig. 3(b), the boundary is shifted to much lower D_{trg}

than that for the PM phase. This shift of the boundary is due to reduction in the V-V hopping integral values.

If we assume $D_{\rm trg} \sim 0.3$ eV, the abrupt change in the a_1 orbital occupation number is expected at the metal-insulator (M-I) transition. Such a large difference in the a_1 orbital occupation number between the metal and insulating phases was indeed inferred from the measurement of the linear dichroism of the V $2p$ X-ray absorption spectrum.[14)] Both the $e^\pi a_1$ to $e^\pi e^\pi$ ratio estimated from the measurement for the AFI phase $e^\pi a_1 : e^\pi e^\pi = 1 : 2$ and the PM phase $e^\pi a_1 : e^\pi e^\pi = 1 : 1$ are well reproduced with $D_{\rm trg} = 0.28$ eV. Since large change in the electronic state are caused by the lattice distortion, i.e., elongation and rotation of the V-V bond of the V ion pair, in this model, it is expected that the lattice distortion is strongly related to the metal-insulator transition. It is also important to mention that there is also large difference in the weight of the d^3d^1 and d^1d^3 configurations between the ground states obtained for the two phases. While the weight is $w(d^3d^1) = w(d^1d^3) = 3.5\%$ for the AFI phase, the weight for the PM phase is 6.9%. Such large increase of the charge fluctuation from the AFI phase to the PM phase in this model again indicates strong connection between the monoclinic distortion and this metal-insulator transition.

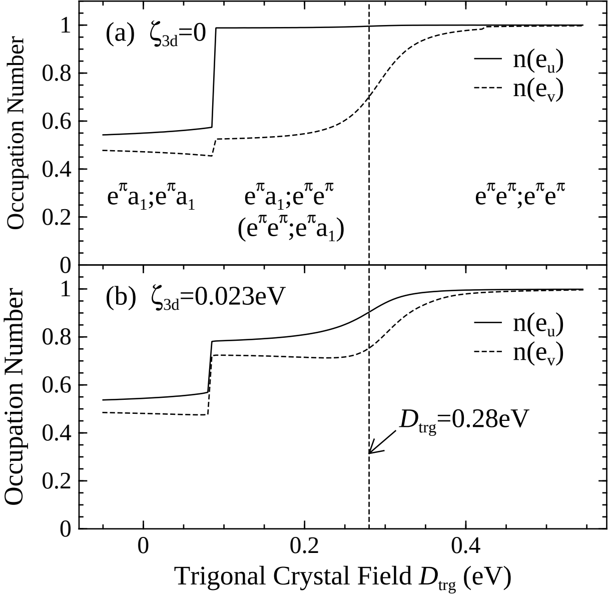

Fig. 4. Trigonal crystal field $D_{\rm trg}$ dependence of the e_u (e_v) orbital occupation number $n(e_u)$ ($n(e_v)$) per V ion in the ground state without (a) and with (b) the $3d$ spin-orbit interaction for the AFI phase are shown. The vertical line is positioned at $D_{\rm trg} = 0.28$ eV, where the ground state gives the ratio $e^\pi a_1 : e^\pi e^\pi = 1 : 2$ deduced from the XAS experiments for the AFI phase.

To see the effects of the $3d$ spin-orbit interaction on the ground state wavefunction in the AFI phase much clearly, in Fig. 4, $D_{\rm trg}$ dependence of the e_u and e_v orbital occupation numbers $n(e_u)$ and $n(e_v)$ per V ion without (a) and with (b) the $3d$ spin-orbit interaction are shown for the AFI phase. There is large difference between the two cases. For $0.09 < D_{\rm trg} < 0.25$, without the spin-orbit interaction, the occupation numbers are $n(e_u) \sim 1$ and $n(e_v) \sim 1/2$ and this shows that the ground state is mainly dominated by the $e^\pi_u a_1; e^\pi_u e^\pi_v$ ($e^\pi_u e^\pi_v; e^\pi_u a_1$) configuration. This also indicates that the monoclinic distortion will induce the ferro V$_2$ molecular orbital order in the AFI phase, which is proposed by Mila *et al.*[18,19)] On the other hand, in the same parameter range, with the spin-orbit interaction, the occupation numbers are $n(e_u) \sim n(e_v) \sim 3/4$ and both two kinds of the configurations $e^\pi_u a_1; e^\pi_u e^\pi_v$ and $e^\pi_v a_1; e^\pi_u e^\pi_v$ are almost in equal weight. As was discussed before, this is because the strong coupling between the spin and orbital degeneracy and there are no orbital degree of freedom which is independent to the spin degree of freedom in this ground state and thus we do not expect usual Jahn-Teller instability. Around $D_{\rm trg} \sim 0.3$ eV, where the $e^\pi e^\pi; e^\pi e^\pi$ state is mixed with the $e^\pi a_1; e^\pi e^\pi$ ($e^\pi e^\pi; e^\pi a_1$) state, the situation is similar: difference between $n(e_u)$ and $n(e_v)$ is smaller with the spin-orbit interaction than that without the interaction.

The ground state property with the spin-orbit interaction above can be understood more clearly with the aide of an effective Hamiltonian within the limit of large U and $10Dq$. In this limit, the ground state is well described within restricted basis functions $|ge\rangle = |e^\pi_u e^\pi_v; e^\pi_u e^\pi_v\rangle$ and $|g\gamma\rangle = \frac{1}{\sqrt{2}}(|e^\pi_\gamma a_1; e^\pi_u e^\pi_v\rangle + |e^\pi_u e^\pi_v; e^\pi_\gamma a_1\rangle)$ $(\gamma = u, v)$. For convenience, here, $L' = 1$ pseudo orbital angular momentum operator $\boldsymbol{L}'$ is introduced, where the eigen functions $L'_z|g\ m\rangle = m|g\ m\rangle$ of L'_z are defined by $|g\ m = 0\rangle = -|ge\rangle$ and $|g\ m = \pm 1\rangle = (-{\rm i}|gu\rangle \pm |gv\rangle)/\sqrt{2}$. The effective Hamiltonian can be expressed using $\boldsymbol{L}'$ and the $S^{\rm T} = 2$ total spin operator $\boldsymbol{S}^{\rm T}$ of the V ion pair as

$$H_{\rm eff} = -\lambda\{S^{\rm T}_z L'_z + \sqrt{2}(S^{\rm T}_x L'_x + S^{\rm T}_y L'_y)\} + \Delta {L'}^2_z + \sqrt{2}C_{\rm A}(e^\pi_v, a_1)(L'_z L'_y + L'_y L'_z), \qquad (3)$$

where $\lambda = \zeta_{3d}/4$ and $\Delta = D_{\rm trg} - \{(dd\sigma)^2 + (dd\pi/3)^2\}/(U' - J)$. Note that there are relations between the real total orbital angular momentum operator $\boldsymbol{L}$ and $\boldsymbol{L}'$ within this restricted basis: $L_x = -\sqrt{2}L'_x$, $L_y = -\sqrt{2}L'_y$ and $L_z = -L'_z$. If $C_{\rm A}(e^\pi_v, a_1) = 0$, the system has uniaxial anisotropy and when $\Delta < -2\lambda$, the z-axis is the magnetic easy axis and the ground state is $|g\pm\rangle = |gm = \pm 1\rangle|S^{\rm T}_z = \pm 2\rangle$, which is identical to that in eq. (2). On the other hand, for $\Delta > -2\lambda$, the x-y plane is the magnetic easy plane. With finite $C_{\rm A}(e^\pi_v, a_1)$, the term $(L'_z L'_y + L'_y L'_z)$ causes hybridization between $|ge\rangle$ and $|gu\rangle$ and this rotate the magnetic easy axis from the z-axis toward the y-axis. The ground state can be regarded as magnetic doublet state having their magnetic moments along this easy axis with opposite directions in each other, although breaking of the rotational symmetry around this easy axis causes a small energy splitting < 0.5 meV between these lowest two eigen states.

2.4 Magnetic anisotropy

As was discussed in the previous subsection the admixture of the $e^\pi e^\pi; e^\pi e^\pi$ state in the ground state lead to rotation of the magnetic easy axis. To study such magnetic properties of the ground state, a molecular field $H_{\rm M}$ with a canting angle $\theta_{\rm M}$ with respect to the z-axis in the

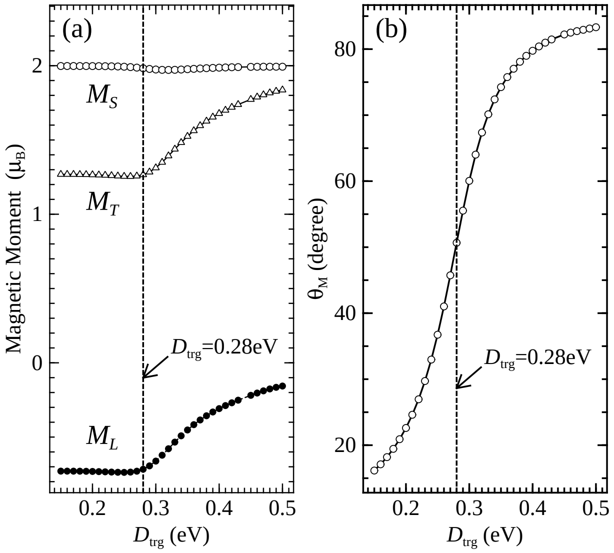

Fig. 5. Sizes of the spin M_S, orbital M_L and total M_T magnetic moments (a) and the canting angle of the total magnetic moment from the z-axis θ_M (b) as a function of the trigonal crystal field D_{trg}.

y-z plane was further applied in the V ion pair model:

$$H_{mol} = H_M \sum_{\gamma} \{ \cos\theta_M (a^{\dagger}_{A\gamma\uparrow} a_{A\gamma\uparrow} - a^{\dagger}_{A\gamma\downarrow} a_{A\gamma\downarrow}) \\ -\mathrm{i}\sin\theta_M (a^{\dagger}_{A\gamma\uparrow} a_{A\gamma\downarrow} - a^{\dagger}_{A\gamma\downarrow} a_{A\gamma\uparrow}) \}.$$

In the calculation, the molecular field with the magnitude $H_M = 0.01$ eV was adopted and θ_M was chosen so as to give the lowest ground state energy. The magnetic moment is, therefore, parallel to both the magnetic easy axis and the molecular field. Note that the values and direction of the spin and orbital magnetic moments obtained here are not sensitive to the magnitude of the molecular field.

In Fig. 5, the sizes of the spin M_S, orbital M_L and total M_T magnetic moments per V ion (a) and θ_M (b) are shown as a function of D_{trg}. Both the directions of the magnetic moment and the V ion pair are in the y-z plane. For the $e^{\pi}a_1; e^{\pi}e^{\pi}$ $(e^{\pi}e^{\pi}; e^{\pi}a_1)$ ground state, the direction of the magnetic moment is parallel to the z-axis (the corundum $\boldsymbol{c}_h$-axis). However, as the weight of the $e^{\pi}e^{\pi}; e^{\pi}e^{\pi}$ configuration in the ground state increases, the magnetic moment is canted toward the y-axis and finally reaches to the y-axis with a pure $e^{\pi}e^{\pi}; e^{\pi}e^{\pi}$ ground state. Note that the V-V bond of the V ion pair is tilted toward opposite direction to the magnetic moment, i.e., toward the negative direction of the y-axis. The large orbital magnetic moment $M_L \sim 0.7\mu_B$ is present in the $e^{\pi}a_1; e^{\pi}e^{\pi}$ $(e^{\pi}e^{\pi}; e^{\pi}a_1)$ ground state. The orbital magnetic moment is about 40% larger than that expected from the ground state wavefunction (see eq. (2)) in the limit of large U and $10Dq$. This deviation is mainly due to the presence of the small weight of configurations with occupied e^{σ} orbitals arising from the $3d$-$3d$ multipole interaction. While M_S remains almost unchanged $M_S \sim 2\mu_B$ as the weight of the $e^{\pi}e^{\pi}; e^{\pi}e^{\pi}$ configuration increases, M_L decreases rapidly. At $D_{trg} = 0.28$ eV, $M_T \sim 1.2\mu_B$ and $\theta_M = 51°$ and these well agree with the values obtained in the neutron diffraction experiments $M_T \sim 1.2\mu_B$ and $\theta_M \sim 71°$.[8)] Strictly speaking, the magnetic moments of the two V ions are slightly tipped out from the y-z plane toward opposite direction in each other. Although the x-component of the magnetic moments is an order of $\sim 0.01\mu_B$, the fact is important for the interpretation of the RXS measurements as will be discussed in § 5.3.

§3. Electron-Lattice Interaction

As was discussed in § 2.3, the pure $e^{\pi}a_1; e^{\pi}e^{\pi}$ $(e^{\pi}e^{\pi}; e^{\pi}a_1)$ ground state has only spin degree of freedom and no orbital degree of freedom is left behind. One would not, therefore, expect usual Jahn-Teller lattice instability in this system. However, in the AFI phase, V_2O_3 exhibits the monoclinic lattice distortion and this indicates that there must be some other kind of lattice instability in this system. Here, it will be shown that such instability indeed appears when the energy of the $e^{\pi}a_1; e^{\pi}e^{\pi}$ $(e^{\pi}e^{\pi}; e^{\pi}a_1)$ and $e^{\pi}e^{\pi}; e^{\pi}e^{\pi}$ states are almost degenerate.

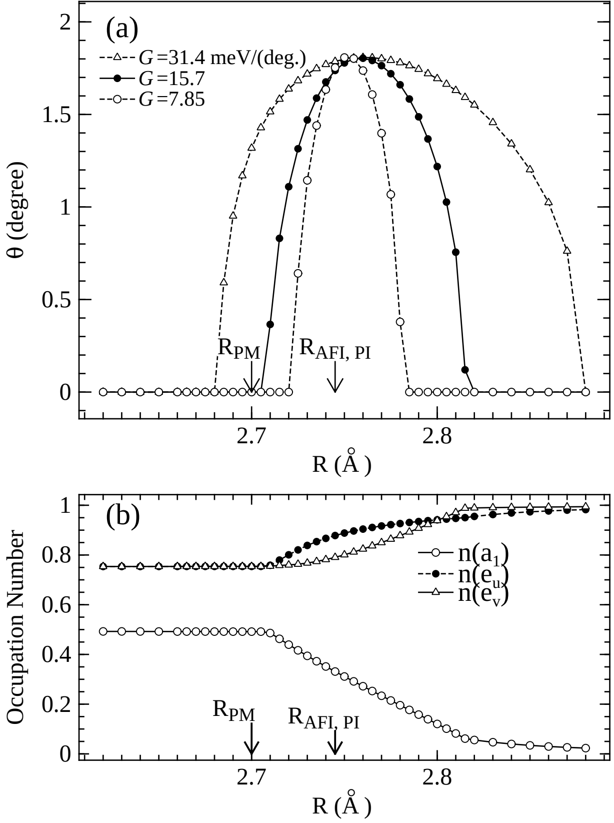

Fig. 6. In (a), tilting angle from the $\boldsymbol{c}_h$-axis as a function of the V-V distance of the V ion pair R is shown for $G = 7.85$, 15.7 and 31.4 meV/(°). $R_{AFI,PI}$ denotes the experimentally observed V-V distance of the V ion pair in both the AFI and PI phases whereas R_{PM} shows that in the PM phase. In (b), the a_1, e_u and e_v orbital occupation numbers calculated with $G = 15.7$ meV/(°) are shown.

In order to discuss interaction between the lattice deformation and the electronic state, here, we consider one V ion pair in the crystal and in addition to the energy of the electronic state discussed in § 2.1, the local lattice deformation energy caused by tilting of the V ion pair is included. The energy of the V ion pair as a function of the polar θ and azimuthal φ angles of the tilting direction would be written in the form:

$$E_{\rm tot}(\theta,\varphi) = E_{\rm elec}(\theta,\varphi) + \frac{K}{2}\theta^2 + F\theta^3 \sin 3\varphi + \ldots, \quad (4)$$

where the first term denotes the ground state energy of the Hamiltonian described in § 2.1 and the second and third terms are the local lattice distortion energies.

Instead of including $F\theta^3 \sin 3\varphi$ and much higher order trigonal potential terms of the lattice deformation, for simplicity, we consider the lowest term $\frac{K}{2}\theta^2$ only and assume that tilting occurs only to the restrict directions of $\varphi = -\frac{\pi}{2}, -\frac{\pi}{2} \pm \frac{2\pi}{3}$, where displacements of each V ion of the pair is parallel to one of the three V-V bond in the honeycomb layer. As a result, the V-V bond along this direction is elongated and those in the other two directions contract. Note that this tilting direction is consistent with that observed in the monoclinic lattice distortion in the AFI phase. In such lattice distortion, both the e^π_u and e^π_v orbitals can be hybridized with the a_1 orbital and corresponding low symmetry crystal field parameters, which are linear functions in θ for small lattice distortion, can be written in the form:

$$C_{\rm A}(e^\pi_u, a_1) = \frac{G\theta}{\sqrt{2}}\cos\varphi, \quad C_{\rm A}(e^\pi_v, a_1) = \frac{G\theta}{\sqrt{2}}\sin\varphi. \quad (5)$$

In the calculation, $D_{\rm trg} = 2.8$ eV was adopted and the V-V distance R dependence for the *d-d* hopping integrals $dd\sigma, dd\pi \propto 1/R^5$ was assumed.

In Fig. 6, the tilting angle at the minimum of $E_{\rm tot}$ as a function of the V-V distance of the V ion pair R is shown for three different crystal fields $G = 7.85$ (open circles), 15.7 (closed circles) and 31.4 meV/(°) (triangles). The coefficient K was chosen so that maximum tilting angle is 1.8° and those for $G = 7.85$, 15.7 and 31.4 meV/(°) are $K = 2.60$, 6.50 and 15.7 meV/(°)^2, respectively. The V-V distances $R_{\rm AFI,PI}$ and $R_{\rm PM}$ are the experimentally observed values in the insulating phases and in the PM phase, respectively.[2)] The rotation of the V ion pair occurs only when the energy of the two kinds of the states $e^\pi a_1; e^\pi e^\pi$ $(e^\pi e^\pi; e^\pi a_1)$ and $e^\pi e^\pi; e^\pi e^\pi$ are nearly degenerate and takes the maximum value around $R = 2.750$ Å, where the two kinds of the states are just degenerate. Note that the energy difference between the two can be given by $\sim D_{\rm trg} - \{(dd\sigma)^2 + (dd\pi/3)^2\}/(U' - J)$.

This instability toward the lattice distortion can be explained by the similar mechanism to the Jahn-Teller effects. If we include the lattice distortion energy, the effective Hamiltonian eq. (3) generalized for the V ion pair with an arbitrary tilting angle (θ,φ) can be written as

$$\begin{aligned} H_{\rm eff} = &-\lambda\{S^{\rm T}_z L'_z + \sqrt{2}(S^{\rm T}_x L'_x + S^{\rm T}_y L'_y)\} + \Delta L'^2_z \\ &+ G\theta\{\cos\varphi(L'_z L'_x + L'_x L'_z) + \sin\varphi(L'_z L'_y + L'_y L'_z)\} \\ &+ \frac{K}{2}\theta^2 + F\theta^3 \sin 3\varphi + \ldots. \qquad (6) \end{aligned}$$

When the energies of the these two kind of states $|ge\rangle$ and $|g\gamma\rangle$ $(\gamma = u, v)$ are degenerate or nearly degenerate, the term linear in θ, which couples the states $|ge\rangle$ and $|g\gamma\rangle$, causes rotation of the V ion pair in the same way as the Jahn-Teller effects. The condition for instability toward tilting is approximately obtained for small λ and $|F|$ as $|\Delta| < 2G^2/K$.

Since the energy gain from this electron-lattice interaction is maximum at the V-V distance where the energies of the two kinds of the states are nearly degenerate, if this mechanism is the cause of the monoclinic distortion in the AFI phase, the V-V distance of the pair in this phase should be at this distance. Indeed, the value $R = 2.755$ Å giving the maximum tilting angle is very near to the value $R_{\rm AFI,PI} = 2.745$ Å, where the V $2p$ XAS experimental results on the $e^\pi e^\pi$ and $e^\pi a_1$ configuration ratio for the AFI phase $e^\pi a_1 : e^\pi e^\pi = 1 : 2$ is reproduced.[14)] The monoclinic lattice distortion in the AFI phase thus can be understood by this mechanism. On the other hand, the V-V distance is much shorter in the PM phase $R_{\rm PM} \sim 2.700$ Å and if $|G| < 16$ meV, the lattice instability does not occur at this distance. In this situation, pure $e^\pi a_1; e^\pi e^\pi$ $(e^\pi e^\pi; e^\pi a_1)$ state is expected in this phase. This also agrees with the V $2p$ XAS experiment, where $e^\pi a_1 : e^\pi e^\pi = 1 : 1$ is obtained in the PM phase.

Although the experimentally observed V-V distance is the same to that for the AFI phase, in the PI phase, no monoclinic lattice distortion has been found. This can be explain as follows. In the PI phase, each V ion pair is also tilted from the $\boldsymbol{c}_h$-axis similar to the AFI phase. However, their tilting directions are disordered and fluctuate among the three stable directions $\varphi = -\frac{\pi}{2}, -\frac{\pi}{2} \pm \frac{2\pi}{3}$, resulting in no monoclinic lattice distortion. This assumption is consistent with the V $2p$ XAS experimental results, where the weight of the $e^\pi e^\pi$ configuration is larger than that of the $e^\pi a_1$ configuration both in the PI and AFI phases in their initial state, indicating admixture of the $e^\pi e^\pi; e^\pi e^\pi$ configuration. If this assumption is correct, the AFI → PI transition is accompanied by order to disorder transition in the tilting directions of the V ion pairs. As will be discussed in the next section, this ordering of the tilting direction in the AFI phase can be explained by a model in which this local lattice distortion and the magnetic exchange interaction between the V ion pairs are considered.

From above discussion, it is expected that there are at least two local minima for the free energy of the real system as a function of the V-V distance of the pair. One is positioned at $R_{\rm PM} \sim 2.700$ Å, where the energy difference of the two kinds of the state $e^\pi a_1; e^\pi e^\pi$ and $e^\pi e^\pi; e^\pi e^\pi$ is large and thus no electron-lattice coupling takes place, and the other one is located at $R_{\rm AFI,PI} \sim 2.745$ Å, where energy of the two kinds of the states is degenerate and Jahn-Teller like lattice distortion is the cause of the energy lowering at this V-V distance. The expansion of the V-V distance in the AFI and PI phases as compared to that in the PM phase can be understood as a consequence of the large change in the $3d$ orbital occupation owing to the tilting of the V ion pair. Since mixture of the $e^\pi e^\pi; e^\pi e^\pi$ state in the ground state reduces electron occupation of the a_1 orbital, which point toward the direction of the V-V bond, the nuclear charges of the V ions of the pair is much less screened by the $3d$ electron in the V-V bond direction, resulting in elongation of the V-V bond.

Since both in the AFI and PI phases, the electron-lattice coupling strongly influences the orbital occupation and charge fluctuation, the PM → AFI and PM → PI transitions can not be regarded as usual Mott transition. In § 2.3, it is found that when the lattice distortion occurs, charge fluctuation between the two V ions is strongly suppressed. The expansion of the V-V distance and resultant reduction of the d-d hybridization strength due to this electron-lattice coupling in the insulating phases is probably the main cause of this metal-insulator transition.

§4. Magnetic Interaction between V Ion Pairs

In the previous section, we have discussed about the local lattice distortion effects on the electronic states within individual V ion pairs. Here, we will consider about the exchange interaction between the V ion pairs in its relation with the local lattice distortion in order to discuss the AFI → PI transition observed in $V_{1-x}Cr_xO_3$. The transition is accompanied by the monoclinic to corundum lattice structure transition and in the ultrasonic wave velocities measurements, the C_{44} elastic constant was estimated to soften almost at the transition temperature, showing the nearly second order nature of the transition.[11,12] Contrary to this, in the AFI to PM transition such softening of C_{44} is not observed and the transition is of the first order. In the magnetic thermal-neutron scattering experiments, abrupt change in short range spin correlation function at the transition temperature was observed.[9,10]

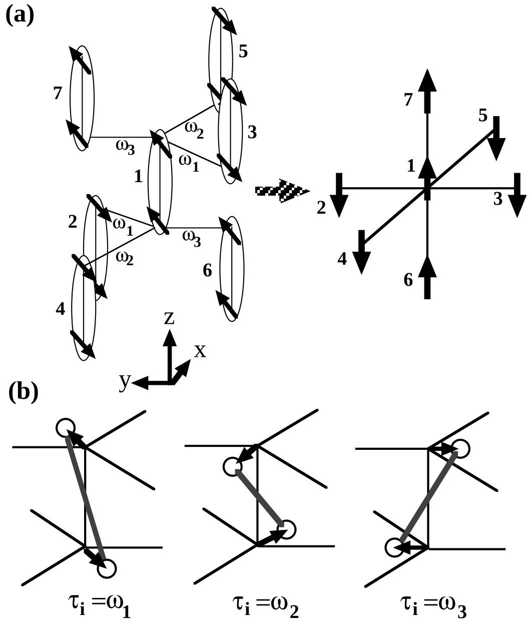

Fig. 7. Mapping of V ion pairs in the corundum lattice on the simple cubic lattice (a) and three possible directions corresponding to $\tau_i = \omega_1$, ω_2 and ω_3 of the tilting of the V ion pair from the $\boldsymbol{c}_{\rm h}$-axis (b) are drawn. On left hand side of Fig. (a), the ovals show the V ion pairs and the allows represent the spin directions of the V ions and on right hand side, the directions of the pseudo spin $\sigma_i = \pm 1$ for V ion pairs are indicated by the arrows. In Fig. (b), the circles and arrows represent the V ions and their displacement due to the tilting of the V ion pair, respectively.

In the AFI phase, the monoclinic lattice distortion and the magnetism are connected, forming unique AF magnetic order. In the monoclinic distortion, all the V ion pairs, which is parallel to the $\boldsymbol{c}_h$-axis in the corundum structure are tilted ∼ 1.8° in the same direction.[2] With this displacement of the V ions, the honeycomb lattice, which has three hold rotational symmetry in the corundum structure, is distorted and V-V bonds in one of the three directions in the layer are elongated and those in the other two directions contract (see Fig. 2). The magnetic moments between two V ions with the elongated V-V bond on the honeycomb lattice are ferromagnetically coupled and those with the contracting V-V bond are antiferromagnetically coupled.

In the theories proposed by Castellani *et al.*[13] and Mila *et al.*,[18,19] the orbital ordering is an essential ingredient for the formation of this unique AF magnetic order in V_2O_3, where exchange coupling constant between the spins of V ions depends on the orbital occupation of the V ions. Rice has pointed out that the abrupt change in the spin correlations at the AFI → PI transition and the short-range spin fluctuations in the PI phase can be explained in the presence of the orbital degree of freedom.[32] Contrary to this, Ezhov *et al.*[17] performed LDA+U band structure calculations and obtained a solution with the unique AF magnetic order as the lowest total energy magnetic state, assuming the monoclinic lattice distortion. Since the orbital occupation in each V ion is $e^\pi e^\pi$, there are no orbital order in this AF magnetic state. In the present theory, since strong coupling between the spin and orbital degrees of freedom due to the spin-orbit interaction, orbital order does not exist in the ground state. Here, it is assumed that the coupling constant of the exchange interaction is a function of the V-V bond length and not depends on the orbital occupation of the V ions.

4.1 Effective spin-lattice Hamiltonian

The effective spin Hamiltonian considered here consists of the exchange interaction between the nearest neighbors of the V ion pairs and the local lattice distortion energy in each V ion pair. Each V ion pair has six nearest neighbors and as depicted in Fig. 7, the network of the V ion pairs can be mapped onto the simple cubic lattice. Two spin directions of the doublet ground state on the i-th V ion pair is projected onto Ising like pseudospin with $\sigma_i = \pm 1$ at the corresponding lattice point i of this simple cubic lattice. The coupling constant of the exchange interaction is assumed to be a function of the displacement of the V-V bond length due to tilting of the V ion pairs. The effective spin Hamiltonian then can be written as

$$H_{\rm S} = -J\sum_{\langle i,j\rangle}\{(\theta_i\boldsymbol{\tau}_i+\theta_j\boldsymbol{\tau}_j)\cdot\boldsymbol{l}_{ij}-C\}\sigma_i\sigma_j+\sum_i\Big(\frac{K}{2}{\theta_i}^2-G\theta_i\Big),$$

where the first term represents the exchange interaction between the pseudo-spins of the V ion pairs and the second term describes the local lattice distortion energy in each V ion pairs. $\theta_i \geq 0$ represents tilting angle of the i-th V ion pair and two dimensional unit vector $\boldsymbol{\tau}_i$ denotes the direction of the tilting projected on the honeycomb layer. Here, we assume that each V ion pair is tilted in such a direction that each V ion in both end is parallel to one of the three V-V bond in the honeycomb layer and elongates this V-V bond. $\boldsymbol{\tau}_i$ is, therefore, in one of these three directions: $\boldsymbol{\omega}_1 = (\sqrt{3}/2, 1/2)$, $\boldsymbol{\omega}_2 = (-\sqrt{3}/2, 1/2)$ or $\boldsymbol{\omega}_3 = (0, -1)$. $\boldsymbol{l}_{ij} = \boldsymbol{\omega}_1$, $\boldsymbol{\omega}_2$ or $\boldsymbol{\omega}_3$ indicates the direction of the V-V bond between the i- and j-th V ion pairs. Thus, the term $(\theta_i \boldsymbol{\tau}_i + \theta_j \boldsymbol{\tau}_j) \cdot \boldsymbol{l}_{ij}$ is proportional to the elongation of the V-V distance between the i- and j-th V ion pairs.

The AF magnetic order observed in V_2O_3 corresponds to the C-type AF magnetic order in this model, where the nearest neighbor spins along one of the lattice line in the simple cubic lattice are coupled ferromagnetically and those along the other two are antiferromagnetically coupled (see Fig. 7 (a)). For this AF magnetic order, the energy per V ion pair is easily obtained as a function of a uniform distortion $\theta = \theta_i$

$$E(\theta) = -|J|C - (G + 4|J|)\theta + \frac{K}{2}\theta^2$$

and the energy has minimum at $\theta_{\min} = \frac{G+4|J|}{K}$

$$E(\theta_{\min}) = -|J|C - \frac{1}{2}\frac{(G + 4|J|)^2}{K}.$$

For this AF magnetic state being stable, the exchange coupling constant $J(2\theta_{\min} - C)$ for the long V-V length should be positive and that for the short V-V length $-J(\theta_{\min} + C)$ should be negative. Thus at least the conditions $J < 0$ and $2\theta_{\min} > C > -\theta_{\min}$ must be satisfied for this AF magnetic state being the ground state.

4.2 AFI to PI phase transition

To study finite temperature properties of this effective Hamiltonian, Monte Carlo simulations were performed with a $24 \times 24 \times 24$ periodic lattice for various values of C. Figure 8 shows the phase diagram as a function of C and $k_{\mathrm{B}}T/|J|$ obtained from the calculation. The adopted value of G is $G = 15.7$ meV$/(^\circ)$ and from the experimental facts $\theta_{\min} \sim 1.8^\circ$ and $T_{\mathrm{N}} \sim 155$ K, the other parameter values are estimated to be $J \sim -4.0$ meV $/(^\circ)$, $K/|J| \sim 3.9$ $(^\circ)^{-1}$ and $G/|J| \sim 3.0$. The solid and dashed lines represent the phase boundaries calculated with $(G/|J| = 3)$ and without $(G/|J| = 0)$ the electron-lattice coupling, respectively. In the range of $-0.3^\circ < C < 2.25^\circ$ as shown in the figure, the low temperature phase is that with the C-type AF magnetic order and the V ion pairs are tilted and ordered in the same direction in this phase (denoted by CO). This phase corresponds to the AFI phase in the real material. The high temperature phase is paramagnetic and the tilting direction of the V ion pairs are disordered (denoted by PD) and this phase corresponds to the PI phase in the real material. For $C > 1.1^\circ$, there is an intermediate temperature phase with the G-type AF magnetic order, where all the nearest neighbor spins are antiferromagnetically coupled, with disordered tilting directions of the V ion pairs (denoted by GD). The transition from the CO phase to the PD phase is of the second order whereas the CO → GD and GD → PD phase transitions are of the first order. It is also seen in the figure that the CO phase is further stabilized with the electron-lattice interaction (solid line) than without it (dashed line), showing importance of the interaction for the formation of the C-type AF magnetic order.

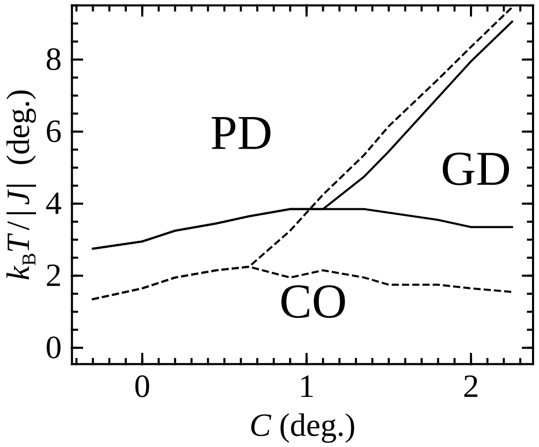

Fig. 8. Phase diagram of the effective spin Hamiltonian for $G/|J| = 3$ (solid line) and $G/|J| = 0$ (dashed line). CO denotes the C-type AF magnetic order with ordered tilting direction of V ion pair. GD and PD are the G-type AF magnetic order and paramagnetic order with disordered tilting direction, respectively.

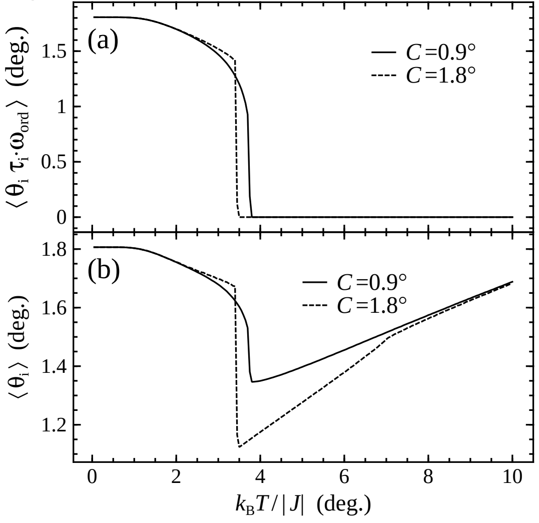

Fig. 9. Order parameter for the tilting of the V ion pairs $\langle \theta_i \boldsymbol{\tau}_i \cdot \boldsymbol{\omega}_{\mathrm{ord}} \rangle$ and the tilting angle $\langle \theta_i \rangle$ as a function of temperature calculated with $C = 0.9^\circ$ (solid line) and $C = 1.8^\circ$ (dashed line).

In Fig. 9, the order parameter of the tilting of V ion pairs $\langle \theta_i \boldsymbol{\tau}_i \cdot \boldsymbol{\omega}_{\mathrm{ord}} \rangle$ and the tilting angle $\langle \theta_i \rangle$ as a function of temperature are shown for $C = 0.9^\circ$ (solid line) and

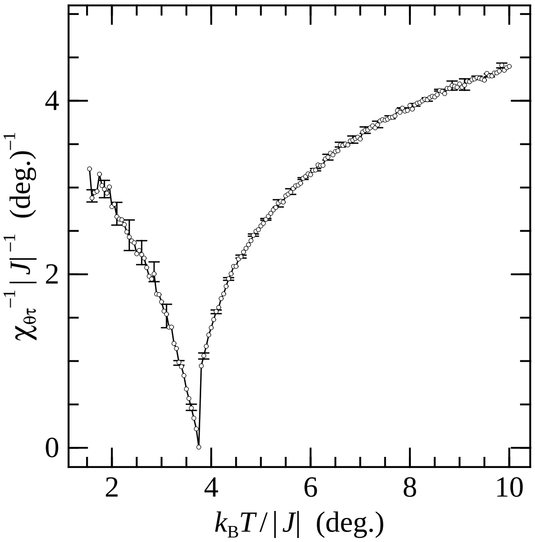

Fig. 10. $1/\chi_{\theta\tau}(T)$ is plotted with error bars for $C = 0.9^\circ$ as a function of temperature.

$C = 1.8^\circ$ (dashed line), where $\boldsymbol{\omega}_{\rm ord}$ is one of the three possible tilting directions $\boldsymbol{\omega}_l$ $(l = 1, 2, 3)$ in which the V ion pairs are ordered. It is seen in the figure that the CO → PD transition is of the second order and the CO → GD transition is of the first order. The tilting angle $\langle\theta_i\rangle$ in the PD phase is much larger than that in the GD phase, showing stronger dynamic lattice distortion in the PD phase. The order parameter of the tilting $\langle\theta_i\boldsymbol{\tau}_i\cdot\boldsymbol{\omega}_{\rm ord}\rangle$ is expected to be approximately proportional to the degree of the monoclinic lattice distortion corresponding to the strain e_4 (see Fig. 2). The reciprocal of the quantity defined by $\chi_{\theta\tau}(T) = (\langle\theta_i\boldsymbol{\tau}_i\cdot\boldsymbol{\omega}_{\rm ord}\rangle^2 - \langle(\theta_i\boldsymbol{\tau}_i\cdot\boldsymbol{\omega}_{\rm ord})^2\rangle)/k_BT$ is therefore proportional to the elastic stiffness constant C_{44}. In Fig. 10(c), $1/\chi_{\theta\tau}(T)$ is plotted as a function of temperature. Both above and below T_N, $1/\chi_{\theta\tau}$ decreases as temperature approaches to T_N. Since the transition is of the second order, the value of $1/\chi_{\theta\tau}$ is zero just at T_N. This temperature dependence of $1/\chi_{\theta\tau}$ is consistent with the behavior of C_{44} observed in ultrasonic wave velocity measurements[11)] and also in neutron scattering experiments[12)] on Cr doped V_2O_3, where C_{44} softens with decreasing temperature in the PI phase and approaches zero near the PI → AFI transition temperature.

In Table III, spatial correlation functions $\langle\sigma_i\sigma_j\rangle$ and $\langle\theta_i\boldsymbol{\tau}_i\cdot\theta_j\boldsymbol{\tau}_j\rangle$ between the first, second and third nearest neighbors along a lattice line are listed. Those for temperatures above and below the CO → PD transition calculated with $C = 0.9^\circ$ are shown and for comparison, those for the CO → GD transition calculated with $C = 1.8^\circ$ are also listed. In the CO phase, those along two different lattice lines, parallel and perpendicular to the ferromagnetic plane of the C-type AF order, are shown. In the PD phase, there is short range G-type AF spin correlation, which is consistent with recent neutron scattering experimental results.[9,10)] In addition to this, short range order of tilting directions is also present in this phase. This sudden change in the spin correlation, which is unusual for order-disorder magnetic transition can be explained as follows. In the PD phase, spins and the local lattice deformation are still dynamically coupled and short range C-type AF order with local lattice distortion survives. However, since the short range C-type AF order with three different directions of the ferromagnetic plane are coexistence, we find, in average, the G-type AF spin correlation as seen in Table III. In this way, the abrupt change in the spin correlation functions observed at the AFI → PI transition in the neutron scattering experiments is explained as a result of the simultaneous order to disorder transition of both the tilting directions and spins of the V ion pairs. On the other hand, in the GD phase, since lattice distortion is not required for the stabilization of the G-type AF spin order, the correlation functions between the tilting directions $\langle\theta_i\boldsymbol{\tau}_i\cdot\theta_j\boldsymbol{\tau}_j\rangle$ is almost zero. This is in contrast to the G-type AF spin correlation in the PD phase originating from the short range C-type AF order with the dynamic spin-lattice coupling.

Table III. Spatial correlation functions $\langle\sigma_i\sigma_j\rangle$ and $\langle\theta_i\boldsymbol{\tau}_i\cdot\theta_j\boldsymbol{\tau}_j\rangle$ between the first, second and third nearest neighbors along a lattice line are shown above and below the CO → PD and CO → GD phase transitions. In the CO phase, those along two different lattice lines, parallel and perpendicular to the ferromagnetic plane of the C-type AF order, are listed.

$C = 0.9^\circ,\ K/\vert J\vert = 3.9\ (^\circ)^{-1},\ G/\vert J\vert = 3$ $k_BT/\vert J\vert = 3.65^\circ$ (CO phase)				
	$\langle\sigma_i\sigma_j\rangle$		$\langle\theta_i\boldsymbol{\tau}_i\cdot\theta_j\boldsymbol{\tau}_j\rangle$	
1st	0.678	−0.735	1.21	1.16
2nd	0.670	0.702	1.07	1.09
3rd	0.681	−0.691	1.03	1.05
$k_BT/\vert J\vert = 3.9^\circ$ (PD phase)				
	$\langle\sigma_i\sigma_j\rangle$		$\langle\theta_i\boldsymbol{\tau}_i\cdot\theta_j\boldsymbol{\tau}_j\rangle$	
1st	−0.191		0.170	
2nd	0.141		0.032	
3rd	−0.042		0.005	
$C = 1.8^\circ,\ K/\vert J\vert = 3.9\ (^\circ)^{-1},\ G/\vert J\vert = 3$ $k_BT/\vert J\vert = 3.3^\circ$ (CO phase)				
	$\langle\sigma_i\sigma_j\rangle$		$\langle\theta_i\boldsymbol{\tau}_i\cdot\theta_j\boldsymbol{\tau}_j\rangle$	
1st	0.964	-0.969	2.02	2.12
2nd	0.965	0.966	2.10	2.04
3rd	0.964	-0.965	2.07	2.04
$k_BT/\vert J\vert = 3.8^\circ$ (GD phase)				
	$\langle\sigma_i\sigma_j\rangle$		$\langle\theta_i\boldsymbol{\tau}_i\cdot\theta_j\boldsymbol{\tau}_j\rangle$	
1st	−0.957		−0.001	
2nd	0.955		0.007	
3rd	−0.955		−0.002	

§5. Resonant X-ray Scattering Analysis

Resonant x-ray scattering (RXS) has received much attention recently, as a technique for extracting direct information on magnetic[33,34,35)] and orbital[36)] order. Possibility of observing the orbital ordering in V_2O_3 by RXS have been pointed out by Fabrizio *et al.*[37)] They made predictions on the light polarization and the azimuthal angle of the scattering plane dependence of the resonant Bragg reflection intensities, assuming the orbital order proposed by Castellani *et al.*[13)] The RXS measurements on V_2O_3[20)] and its Cr doped alloys[21)] have been performed by Paolasini *et al.* They insisted that in the AFI phase, there are resonant Bragg reflection peaks arising from the orbital ordering in addition to those caused by the AF magnetic ordering. On the other hand, Lovesey and Knight claimed that all these Bragg peaks can be attributed to the AF magnetic ordering and are associated with the orbital magnetic moment and the octupole moment of a V ion.[23)] In this section, discussion will be mainly focused on these resonant Bragg peaks, especially (111) reflection peak, whose origin is still controversial. It will be shown that the light polarization and the azimuthal angle dependence of the (111) Bragg reflection intensity can be explain within the V ion pair model and is attributed to not the orbital ordering but the antiferro (AF) magnetic ordering.

5.1 $1s \rightarrow 4p$ dipole X-ray scattering process

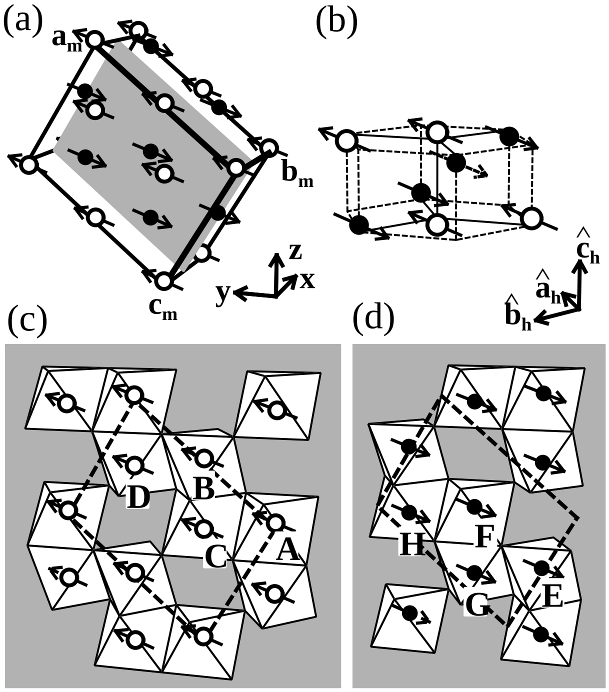
(a)
$\mathbf{a_m}$
$\mathbf{b_m}$
$\mathbf{c_m}$
z
y
x
(b)
$\hat{\mathbf{c}}_\mathbf{h}$
$\hat{\mathbf{a}}_\mathbf{h}$
$\hat{\mathbf{b}}_\mathbf{h}$
(c)
D
B
C
A
(d)
H
F
G
E

Fig. 11. Antiferromagnetic and crystal structures of V_2O_3 in the AFI phase. The white and black circles denote V ions and the arrows indicate direction of their magnetic moments. In (a), the monoclinic unit cell and the magnetic structure are shown. The magnetic moments are ferrromagnetically coupled in each monoclinic (010) layer, altering their direction between adjacent layers. The V ion pair and neighboring six V ions are depicted in (b). In (c) and (d), V ions belonging to two different (010) layers are separately depicted with surrounding oxygen octahedra.

In this subsection, we will discuss the $1s \rightarrow 4p$ dipole process, which is dominant process in the RXS at the V K-edge absorption region. The x-ray scattering amplitude $f_{\mathrm{DD}}(\omega)$ is expressed as

$$f_{\mathrm{DD}}(\omega) = \sum_{l} e^{\mathrm{i}(\boldsymbol{q}-\boldsymbol{q}')\cdot \boldsymbol{R}_l}(\boldsymbol{\varepsilon}'^{*} \cdot F^l(\omega)\boldsymbol{\varepsilon}), \qquad (7)$$

where $\boldsymbol{q}$ and $\boldsymbol{\varepsilon}$ are the wave vector and the polarization vector for the the incoming photon, $\boldsymbol{q}'$ and $\boldsymbol{\varepsilon}'$ are those for the outgoing photon and $\boldsymbol{R}_l$ denotes position of the l-th V ion site.

Here, the 3×3 tensor $F^l(\omega)$ is defined by

$$F^l(\omega) = q^2 \langle \mathrm{g}|\boldsymbol{P}\frac{1}{E_g + \omega - H_{\mathrm{m}} + \mathrm{i}\Gamma_{\mathrm{m}}/2}{}^t\boldsymbol{P}|\mathrm{g}\rangle, \qquad (8)$$

where $|g\rangle$ and E_g are the ground state wave functions and its energy, H_{m} and Γ_{m} are the Hamiltonian and a life-time term for the intermediate state reached by the $1s \rightarrow 4p$ transition and $\boldsymbol{P} = e\boldsymbol{r}$ is the electric dipole moment operator. Since delocalized feature of the $4p$ orbital, the intermediate-state-multiplet dependence of RXS is not expected to be important. Thus, here we will consider the integrated value of $F^l(\omega)$ over the photon energy ω:

$$F^l_{i,j} = \int F^l_{i,j}(\omega)\, d\omega. \qquad (9)$$

Note that $F^l_{x,x}$, $F^l_{y,y}$ and $F^l_{z,z}$ correspond to the $1s \rightarrow 4p$ dipole transition probabilities integrated by ω at site l with x-, y- and z- linearly polarized light, respectively.

Before discussing rather complicate RXS in V_2O_3, first of all, let us consider the most simplest antiferromagnet, where the unit cell with one magnetic ion site in the absence of magnetic order is doubled by the presence of the antiferromagnetic order and two magnetic sublattices A and B with opposite direction of the magnetic moment in each other are assumed. In this case, F^l for an ion site belongs to the sublattice A (here we denote it by F^{A}) can be obtained from that belongs to the sublattice B (denoted by F^{B}) by replacing the ground state wavefunction $|g\rangle$ in eq. (8) with $\Theta T|g\rangle$, where Θ represents the time reversal operator and T denotes the translation operator, which transforms ion sites belong to the sublattice A into those belong to the sublattice B. This immediately leads to the relation:

$$F^{\mathrm{A}} = F^{\mathrm{B}*}.$$

For resonant Bragg reflection corresponding to the antiferromagnetic order, the integrated scattering amplitude f_{DD} is

$$\begin{aligned} f_{\mathrm{DD}} &= \frac{N}{2}\sum_{i,j}(F^{\mathrm{A}}_{i,j} - F^{\mathrm{A}*}_{i,j})\varepsilon_i\varepsilon'_j \\ &= \mathrm{i}N\{(\varepsilon_x\varepsilon'_y - \varepsilon_y\varepsilon'_x)\mathrm{Im}F^{\mathrm{A}}_{x,y} + (\varepsilon_y\varepsilon'_z - \varepsilon_z\varepsilon'_y)\mathrm{Im}F^{\mathrm{A}}_{y,z} \\ &\quad + (\varepsilon_z\varepsilon'_x - \varepsilon_x\varepsilon'_z)\mathrm{Im}F^{\mathrm{A}}_{z,x}\}, \qquad (10) \end{aligned}$$

where N denotes the number of the magnetic ion sites. $\mathrm{Im}F^{\mathrm{A}}_{x,y}$ can be written as

$$\mathrm{Im}F^{\mathrm{A}}_{x,y} = \frac{1}{2\mathrm{i}}(F^{\mathrm{A}}_{+1} - F^{\mathrm{A}}_{-1}),$$

where $F^{\mathrm{A}}_{\pm 1}$ are integrated transition probabilities of the $1s \rightarrow 4p$ dipole transition with plus and minus helicity light injected along the z-axis for an ion site belongs to the sublattice A. Carra *et al.* have proposed a sum rule for the core-level x-ray absorption spectra with the circularly polarized light.[38)] From the sum rule, it is easy to find that the quantity $F^{\mathrm{A}}_{+1} - F^{\mathrm{A}}_{-1}$ is proportional to the z-component of the orbital moment of the $4p$ orbital $\langle L^{4p}_z \rangle$ for a magnetic ion site belongs to the sublattice

A in the ground state. Similarly, the quantities $\mathrm{Im}F^{\rm A}_{y,z}$ and $\mathrm{Im}F^{\rm A}_{z,x}$ are proportional to the x- and y-components of the $4p$ orbital angular momenta $\langle L^{4p}_x\rangle$ and $\langle L^{4p}_y\rangle$, respectively. The integrated amplitude $f_{\rm DD}$ is, therefore, proportional to $(\boldsymbol{\varepsilon}\times\boldsymbol{\varepsilon}')\cdot\langle\boldsymbol{L}^{4p}\rangle$.

In Fig. 11, the magnetic and crystal structures in the AFI phase are shown. The black and white circles are the V ion sites and the arrows indicate the direction of their magnetic moments. There are eight different V ion sites in the monoclinic unit cell shown in Fig. 11(a). In (b) and (c), two different (010) magnetic layers are separately drawn, and the eight V ion sites are labeled A to H. The integrated scattering amplitude $f_{\rm DD}(h,k,l)$ of RXS at a (h,k,l) Bragg reflection can be written in the form:

$$\begin{aligned} f_{\rm DD}(h,k,l)=\frac{N}{8}\sum_{i,j}\varepsilon_i\varepsilon'_j\big[&\{F^{\rm A}_{i,j}+(-)^{h+k+l}F^{\rm F}_{i,j}\}\\ &+\{F^{\rm B}_{i,j}+(-)^{h+k+l}F^{\rm E}_{i,j}\}(-)^h\\ &+\{F^{\rm C}_{i,j}+(-)^{h+k+l}F^{\rm H}_{i,j}\}e^{{\rm i}\alpha}\\ &+\{F^{\rm D}_{i,j}+(-)^{h+k+l}F^{\rm G}_{i,j}\}(-)^h e^{{\rm i}\alpha}\big], \end{aligned}\tag{11}$$

where $\alpha\sim -4\pi(hx+lz)$. $x\sim$0.3438 and $z\sim$0.2991 are the position parameters of the V ions.[2)] If we assume the antiferromagnetic structure above, the system is invariant under the symmetry operation $\{\Theta|\frac{1}{2}(\boldsymbol{a}_m+\boldsymbol{b}_m+\boldsymbol{c}_m)\}$ and by this operation, the V ion sites A, B, C and D are transformed into the sites F, E, H and G, respectively and as we have discussed above, relations $F^{\rm A}=F^{\rm F*}$, $F^{\rm B}=F^{\rm E*}$, $F^{\rm C}=F^{\rm H*}$ and $F^{\rm D}=F^{\rm G*}$ are satisfied. Similarly, the V ion sites A, C, E and G are transformed into the sites B, D, F and H by the $I2/a$ space group symmetry operation $\{\sigma_{\rm h}|\frac{1}{2}\boldsymbol{a}_m\}$ and relations $F^{\rm A}=F^{\rm B}$, $F^{\rm C}=F^{\rm D}$, $F^{\rm E}=F^{\rm F}$ and $F^{\rm G}=F^{\rm H}$ are obtained. Using above relations among F^l's and also the fact that the operation $\sigma_{\rm h}$ transforms $(\varepsilon_x,\varepsilon_y,\varepsilon_z)$ into $(\varepsilon_x,\varepsilon_y,-\varepsilon_z)$, we obtain the scattering amplitude for the reflections with h =even and $h+k+l$ =odd as

$$\begin{aligned} &f_{\rm DD}(h,k,l)=\\ &\quad\frac{{\rm i}N}{2}\{(\varepsilon_y\varepsilon'_z-\varepsilon_z\varepsilon'_y)(\mathrm{Im}F^{\rm A}_{y,z}+e^{{\rm i}\alpha}\mathrm{Im}F^{\rm C}_{y,z})\\ &\quad+(\varepsilon_z\varepsilon'_x-\varepsilon_x\varepsilon'_z)(\mathrm{Im}F^{\rm A}_{z,x}+e^{{\rm i}\alpha}\mathrm{Im}F^{\rm C}_{z,x})\}. \end{aligned}\tag{12}$$

On the other hand, the scattering amplitude for the reflections with h =odd and $h+k+l$ =odd can be written as

$$\begin{aligned} &f_{\rm DD}(h,k,l)=\\ &\quad\frac{{\rm i}N}{2}(\varepsilon_y\varepsilon'_z-\varepsilon_z\varepsilon'_y)(\mathrm{Im}F^{\rm A}_{y,z}+e^{{\rm i}\alpha}\mathrm{Im}F^{\rm C}_{y,z}). \end{aligned}\tag{13}$$

It is obvious from eqs. (12) and (13) that the amplitudes are zero for the σ-σ scattering, where the polarization vectors $\boldsymbol{\varepsilon}$ and $\boldsymbol{\varepsilon}'$ are perpendicular to the scattering plane and thus are parallel to each other. This is consistent with the experiments, where only vanishingly small intensities of both the (111) and (221) reflections for the σ-σ scattering are observed.[20)] On the other hand, the σ-π scattering, where one of the polarization vectors is perpendicular to the scattering plane and the other is in the plane, is not forbidden scattering and indeed, for the magnetic (221) Bragg reflection, strong RXS are observed in the experiment. The experimental σ-π scattering at the (111) Bragg reflection, however, has only negligible small intensity in the $1s\rightarrow 4p$ excitation energy region. This fact can be explain as follows. Since the direction of the magnetic moment observed in the neutron experiment is almost in the $\boldsymbol{a}_m$-$\boldsymbol{b}_m$ plane, the x-component of the $4p$ orbital angular momentum $\langle L^{4p}_x\rangle$, which is perpendicular to the $\boldsymbol{a}_m$-$\boldsymbol{b}_m$ plane (see Fig. 11), is expected to be zero or small. Because eq. (13) only contains $F^{\rm A}_{y,z}$ and $F^{\rm B}_{y,z}$, which is proportional to $\langle L^{4p}_x\rangle$, the intensity should be almost zero.

5.2 *Interference of* $1s\rightarrow 4p$ *and* $1s\rightarrow 3d$ *processes*

We have discussed the $1s\rightarrow 4p$ dipole RXS. Only the dipole process, the scattering amplitude at the (111) Bragg reflection should be almost zero and thus the $1s\rightarrow 3d$ quadrupole transition expected to be important to explain the sharp peak observed at the prethreshold region. Since V^{3+} ion sites do not have inversion symmetry in $\mathrm{V_2O_3}$, the $4p$ and $3d$ orbitals on the same site can be hybridized in each other and this causes interference between the $1s\rightarrow 4p$ dipole transition and $1s\rightarrow 3d$ quadrupole transition processes.[37)] Because pure $1s\rightarrow 3d$ scattering amplitude is expected to be much smaller than the interference scattering amplitude, here, only this interference scattering process is considered.

The crystal field which causes the hybridization between the $4p$ and $3d$ orbitals in the same V ion site would be written as

$$\begin{aligned} V^l(\boldsymbol{r})=&\pm A_{1,0}r\mathrm{Y}_{1,0}(\Omega)\pm A_{3,0}r^3\mathrm{Y}_{3,0}(\Omega)\\ &\pm A_{3,3}r^3\{\mathrm{Y}_{3,3}(\Omega)-\mathrm{Y}_{3,-3}(\Omega)\}, \end{aligned}\tag{14}$$

where the signs in front of three coefficients $A_{1,0}$, $A_{3,0}$ and $A_{3,3}$ depend on the sites: the plus signs in front of $A_{1,0}$ and $A_{3,0}$ are taken for A, B, E and F sites and the minus signs for the other sites and $+A_{3,3}$ for B, C, E and H sites and $-A_{3,3}$ for the others.

The relative values of the these three parameters were estimated using a $\mathrm{VO_6}$ cluster model and they are $A_{3,3}/A_{3,0}\simeq 0.79$ and $(A_{3,0}\langle 4p|r^3|3d\rangle)/(A_{1,0}\langle 4p|r|3d\rangle)\simeq -0.22$. If we take into account this hybridization as a second order perturbation with respect to V^l, we find for the interference term $f_{\rm DQ}(\omega)$ as

$$\begin{aligned} f_{\rm DQ}(\omega)=&\,{\rm i}q^2\sum_l e^{{\rm i}(\boldsymbol{q}-\boldsymbol{q}')\cdot\boldsymbol{R}_l}\\ &\times\Big[\langle{\rm g}|D(\boldsymbol{\varepsilon}')(\frac{V^l}{\Delta_{4p\text{-}3d}})\frac{1}{E_g+\omega-H_{\rm m}+{\rm i}\frac{\Gamma_{\rm m}}{2}}Q(\boldsymbol{\varepsilon},\boldsymbol{q})|{\rm g}\rangle\\ &-\langle{\rm g}|Q(\boldsymbol{\varepsilon}',\boldsymbol{q}')\frac{1}{E_g+\omega-H_{\rm m}+{\rm i}\frac{\Gamma_{\rm m}}{2}}(\frac{V^l}{\Delta_{4p\text{-}3d}})D(\boldsymbol{\varepsilon})|{\rm g}\rangle\Big], \end{aligned}\tag{15}$$

where $|{\rm g}\rangle$ and E_g are the ground state wavefunction and its energy, $D(\boldsymbol{\varepsilon})$ and $Q(\boldsymbol{\varepsilon},\boldsymbol{q})$ are the operators for the electric dipole and quadrupole transitions defined by $D(\boldsymbol{\varepsilon})=e(\boldsymbol{\varepsilon}\cdot\boldsymbol{r})$ and $Q(\boldsymbol{\varepsilon},\boldsymbol{q})=e(\boldsymbol{r}\cdot\boldsymbol{\varepsilon})(\boldsymbol{r}\cdot\boldsymbol{q})$, $\Delta_{4p\text{-}3d}$ is the energy difference between the $4p$ and $3d$ levels and $H_{\rm m}$ and $\Gamma_{\rm m}$ are the Hamiltonian and the life-time term for the intermediate state reached by the $1s \to 3d$ excitation from the initial state.

The term $1/(E_g + \omega - H_{\rm m} + {\rm i}\Gamma_{\rm m}/2)$ would be approximately replaced by $-{\rm i}\pi \sum_\mu \delta(E_g + \omega - E_\mu)|\mu\rangle\langle\mu|$, where $H_{\rm m}|\mu\rangle = E_\mu|\mu\rangle$ and with this approximation, the RXS amplitude integrated by ω over $1s \to 3d$ excitation energy region can be written as

$$\begin{aligned}&\int_{1s\to3d} f_{\rm DQ}(\omega)\, d\omega\\ &\sim \pi(eq)^2 \frac{\langle 1s|r|4p\rangle\langle 1s|r^2|3d\rangle}{\Delta_{4p\text{-}3d}}\\ &\times \sum_{l,m,m'} e^{{\rm i}(\boldsymbol{q}-\boldsymbol{q}')\cdot\boldsymbol{R}_l}\langle g|\sum_\sigma a_{lm\sigma}a^\dagger{}_{lm'\sigma}|g\rangle\\ &\times \Big[D^*_m(\boldsymbol{\varepsilon}')V^l_{m,m'}Q_{m'}(\boldsymbol{\varepsilon},\boldsymbol{q}) - Q^*_m(\boldsymbol{\varepsilon}',\boldsymbol{q}')V^{l*}_{m',m}D_{m'}(\boldsymbol{\varepsilon})\Big],\end{aligned} \tag{16}$$

where $V^l_{m,m'} = \int R_{4p}(r)Y^*_{1m}(\Omega)V^l(\boldsymbol{r})R_{3d}(r)Y_{2m'}(\Omega)\, d\boldsymbol{r}$ and $a^\dagger_{lm\sigma}$ denotes creation operator of an electron on the $3d$ orbital with magnetic m and spin σ quantum numbers on site l. D_m and Q_m are coefficients of the spherical expansions of the transition operators

$$D(\boldsymbol{\varepsilon}) = er\sum_{m=-1}^{1} D_m(\boldsymbol{\varepsilon})Y_{1m}(\Omega)$$

$$Q(\boldsymbol{\varepsilon},\boldsymbol{q}) = er^2\sum_{m=-2}^{2} Q_m(\boldsymbol{\varepsilon},\boldsymbol{q})Y_{2m}(\Omega)$$

and they are given by

$$D_{\pm1} = \sqrt{\frac{4\pi}{3}}\frac{\mp\varepsilon_x + {\rm i}\varepsilon_y}{\sqrt{2}}, \qquad D_0 = \sqrt{\frac{4\pi}{3}}\varepsilon_z,$$

$$Q_{\pm2} = \sqrt{\frac{2\pi}{15}}\big\{(q_x\varepsilon_x - q_y\varepsilon_y) \mp {\rm i}(q_x\varepsilon_y + q_y\varepsilon_x)\big\},$$

$$Q_{\pm1} = \sqrt{\frac{2\pi}{15}}\big\{\mp(q_z\varepsilon_x + q_x\varepsilon_z) + {\rm i}(q_y\varepsilon_z + q_z\varepsilon_y)\big\},$$

$$Q_0 = \sqrt{\frac{4\pi}{5}}q_z\varepsilon_z.$$

The procedure of the calculations is following. Eight V ion sites (A to H in Fig. 11) in the monoclinic unit cell was considered to be four independent V ion pairs. For each of them, the ground state wavefunction was calculated using the V ion pair model described in § 2. In the calculations, molecular field $H_{\rm M} = 0.01$ eV along the magnetic easy axis was applied so to reproduce experimentally observed antiferromagnetic order. Then, from the ground state wavefunctions, the quantity $\langle g|\sum_\sigma a_{lm\sigma}a^\dagger{}_{lm'\sigma}|g\rangle$ were calculated, and using eq. (16), the scattering amplitude was obtained.

5.3 Analysis of the (111) Bragg reflection

Figure 12 shows the theoretical azimuthal angle Φ dependence of the integrated intensities for the (111) Bragg reflection in the AFI phase for various values of $D_{\rm trg}$.

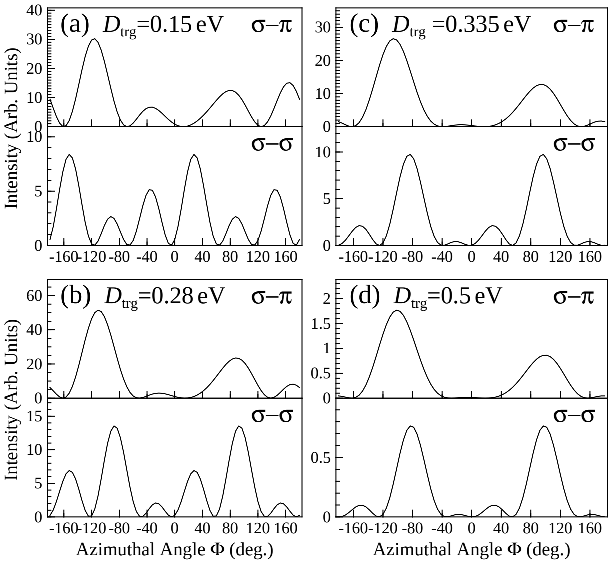

Fig. 12. Azimuthal angle dependence of the integrated intensities for the (111) Bragg reflection in the AFI phase calculated with various values of the trigonal crystal field $D_{\rm trg}$. Intensities for the two porlarization conditions σ-σ and σ-π are shown. The adopted parameter values are $D_{\rm trg} = 0.15$ eV (a), $D_{\rm trg} = 0.28$ eV (b), $D_{\rm trg} = 0.335$ eV (c) and $D_{\rm trg} = 0.5$ eV (d).

The intensities with the two polarization conditions σ-σ and σ-π calculated with the parameters $D_{\rm trg} = 0.15$ eV (a), $D_{\rm trg} = 0.28$ eV (b), $D_{\rm trg} = 0.335$ eV (c) and $D_{\rm trg} = 0.5$ eV (d) are shown. The scattering plane is parallel to the z-axis at $\Phi = 0$. The tilting angle of the magnetic moment $\theta_{\rm M}$ in the ground state with $D_{\rm trg} = 0.15$ eV, 0.28 eV, 0.335 eV and 0.5 eV are $\theta_{\rm M} = 16°$, $51°$, $71°$ and $84°$, respectively.

It is seen in the figure that the azimuthal angle Φ dependence of the scattering intensities are strongly influence by the direction of the orbital magnetic moment. The intensity curve in Fig. 12(c) with $\theta_{\rm M} = 71°$, which is the same angle observed in the neutron diffraction experiment[8] and Fig. 12(b) with $\theta_{\rm M} = 51°$ are most resemble to the experimental intensity curve in ref. 20. On the other hand, the curve in Fig. 12(b), where $\theta_{\rm M} = 16°$ and the ground state is almost pure $e^\pi a_1; e^\pi e^\pi$ $(e^\pi e^\pi; e^\pi a_1)$ state, is very different from experimental one. This indicates that the experimental results are well explained with the $e^\pi e^\pi; e^\pi e^\pi$ and $e^\pi a_1; e^\pi e^\pi$ mixed ground state and consistent with the present theory. It is also important to mention that if the spin-orbit interaction is switched off, the scattering intensity is zero for this reflection, although there exists the molecular ferro-orbital order in the ground state. The reflection, therefore, originates from not the molecular ferro-orbital order but the AF magnetic order.

The scattering intensity is also sensitive to a small x-component of the orbital magnetic moment M_{Lx}. Possibility of the presence of such small x-component of the magnetic moment was pointed out by Moon.[8] M_{Lx} can be induced by the low symmetry crystal field $C_{\rm A}(e^\pi_u, e^\pi_v)$. In Fig. 13(a), Φ dependence of the integrated intensities for the (111) reflection obtained with $C_{\rm A}(e^\pi_u, e^\pi_v) = -0.02$ eV (solid line), 0 eV (dashed line) and 0.02 eV

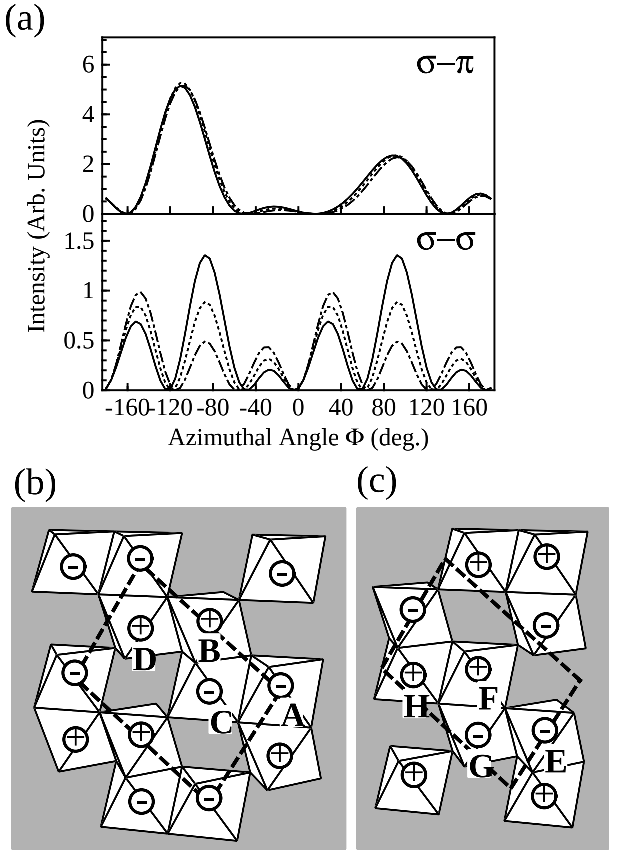

Fig. 13. In (a), azimuthal angle dependence of the integrated intensities for the (111) reflection in the AFI phase calculated with $C_{\rm A}(e^{\pi}_{u}, e^{\pi}_{v}) = -0.02$ eV (solid line), 0.0 eV(dashed line) and 0.02 eV (dotted-dashed line) are shown. In (b) and (c), the same as Fig. 11 (c) and (d), the sign (±) of M_{Lx} on V ions are shown.

(dotted-dashed line) are drawn. $D_{\rm trg} = 0.28$ eV is adopted. In Figs. 13(b) and (c), the sign of M_{Lx} on each V ion for $C_{\rm A}(e^{\pi}_{u}, e^{\pi}_{v}) < 0$ is shown for the two magnetic layers in Figs. 11(b) and (c). For $C_{\rm A}(e^{\pi}_{u}, e^{\pi}_{v}) > 0$, all the signs of M_{Lx} are altered. As seen in the Fig. 13(a), the σ-σ scattering intensity is strongly influenced by the value of $C_{\rm A}(e^{\pi}_{u}, e^{\pi}_{v})$, although the magnitude of M_{Lx} induced by $C_{\rm A}(e^{\pi}_{u}, e^{\pi}_{v}) = \pm 0.02$ eV is an order of $\sim 0.01\mu_{\rm B}$. With $C_{\rm A}(e^{\pi}_{u}, e^{\pi}_{v}) = 0.02$ eV the calculated intensity curve is not resemble to the experimental one whereas with $C_{\rm A}(e^{\pi}_{u}, e^{\pi}_{v}) = -0.02$ eV, good agreement with experimental intensity curve is achieved.

Lovesey and Knight argued that the (111) reflection peak can be explain by pure $1s \to 3d$ quadrupole transition.[23] Contrary to this, in the present theory, the peak is attributed to the interference process of the $1s \to 4p$ dipole and $1s \to 3d$ quadrupole transitions. For comparison, in Fig. 14, Φ dependence of the scattering intensity of the (111) reflection peak obtained with the pure $1s \to 3d$ quadrupole transition instead of the interference process is shown. The intensity curve calculated with $D_{\rm trg} = 0.28$ eV is very different from experimental curve. Results obtained with other parameter values of $D_{\rm trg}$ and $C_{\rm A}(e^{\pi}_{u}, e^{\pi}_{v})$ also does not agree with experimental intensity curve.

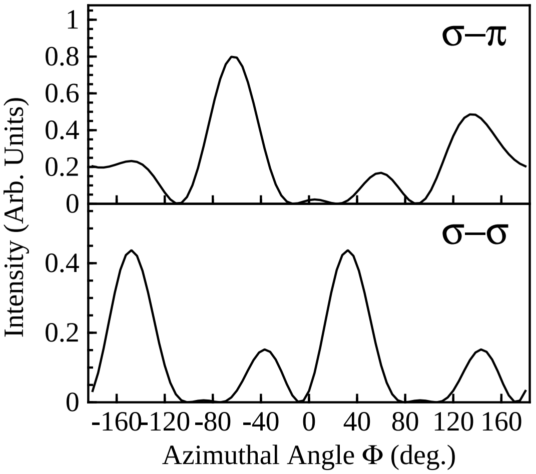

Fig. 14. Azimuthal angle dependence of the integrated intensity for the (111) reflection in the AFI phase calculated with $D_{\rm trg} = 0.28$ eV. The $1s \to 3d$ quadrupole transition instead of the $1s \to 3d$ and $1s \to 4p$ interference process is assumed as for the RXS process.

§6. Linear Dichroism in V 2p XAS

In this section, the dependence of the V 2p XAS spectra on the polarization vector $\boldsymbol{\varepsilon}$ of the light will be discussed. As was mentioned in the previous sections, such experiment was already done by Park *et al.*[14] with the polarization vectors $\boldsymbol{\varepsilon}$ being parallel and perpendicular to the $\boldsymbol{c}_h$-axis. Because of the selection rule of the $2p \to 3d$ dipole transition, the transition probability to the a_1 orbital is larger than that to the e^{π} orbital for $\boldsymbol{\varepsilon}//\boldsymbol{c}_h$, whereas that to the e^{π} orbital is larger for the $\boldsymbol{\varepsilon} \perp \boldsymbol{c}_h$. Thus the difference spectrum is sensitive to the $e^{\pi}a_1$ to $e^{\pi}e^{\pi}$ occupation ratio in the initial state. The ratio was deduced from the experiment using a VO$_6$ cluster model and was found to be $e^{\pi}a_1$: $e^{\pi}e^{\pi} \sim 1:1$ for the PM phase and $e^{\pi}a_1 : e^{\pi}e^{\pi} \sim 1:2$ for the AFI phase.

To verify the present theory, the spectra was calculated using the V ion pair model described in § 2.1. For the initial state, the ground state of the V ion pair model is assumed. For the final state, the configurations $2\underline{p}3d^3; 3d^2$, $2\underline{p}3d^1; 3d^3$ and $2\underline{p}3d^4; 3d^1$ are considered, where $2\underline{p}$ denotes a hole on the V 2p orbital in one of the V ion site. In addition to the interactions considered in the Hamiltonian described in § 2.1, the 3d-2p multipole interaction and the 2p spin-orbit interaction are also included in the calculation of the final states.[39] The $2p \to 3d$ dipole transition is considered as the photoprocess and the intensities of the spectra $I_{\kappa}(\omega)$ as a function of the incident photon energy ω is written as

$$I_{\kappa}(\omega) \propto \sum_{f} \left|\langle f|T_{\kappa}|g\rangle\right|^{2} \delta(E_g + \omega - E_f)$$

$$= \lim_{\delta\to 0} \frac{-1}{\pi} {\rm Im} \langle g|T^{\dagger}_{\kappa} \frac{1}{E_g + \omega - H_f + {\rm i}\delta} T_{\kappa}|g\rangle, \quad (17)$$

where $|f\rangle$, E_f and H_f denote the wavefunction, eigen energy and Hamiltonian of the final state, respectively, T_{κ} represents the $2p \to 3d$ dipole transition operator and κ specifies the polarization direction of the linearly polarized light. The spectra was calculated using the recursion method[40)] and a Lorentzian broadening was further applied the spectra.

The parameters used in the calculations are the same to those listed in Table II and $D_{\rm trg} = 0.28$ eV is adopted. In the final state, there are additional parameters related to the $2p$ core-hole: the $3d$-$2p$ Coulomb repulsion energy $U_{dp} = 3.07$ eV, the $2p$ spin-orbit interaction $\zeta_p = 4.649$ eV, the $3d$-$2p$ Slater integrals $F^2_{dp} = 4.361$ eV, $G^1_{dp} = 3.162$ eV and $G^3_{dp} = 1.797$ eV.

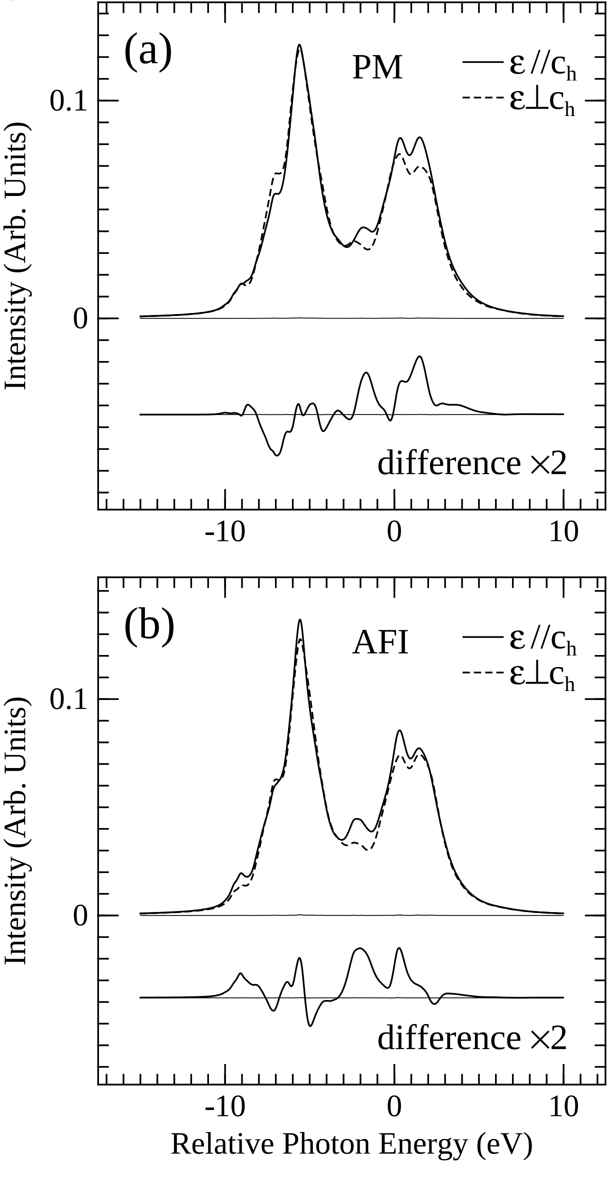

Fig. 15. Theoretical polarization-dependent V $2p$ XAS spectra for V_2O_3 for the PM (a) and AFI (b) phases. The spectra are depicted for two different directions of the polarization vectors $\boldsymbol{\varepsilon}$ of the light: parallel and perpendicular to the $\boldsymbol{c}_h$-axis. The difference spectra are also shown below in each panel.

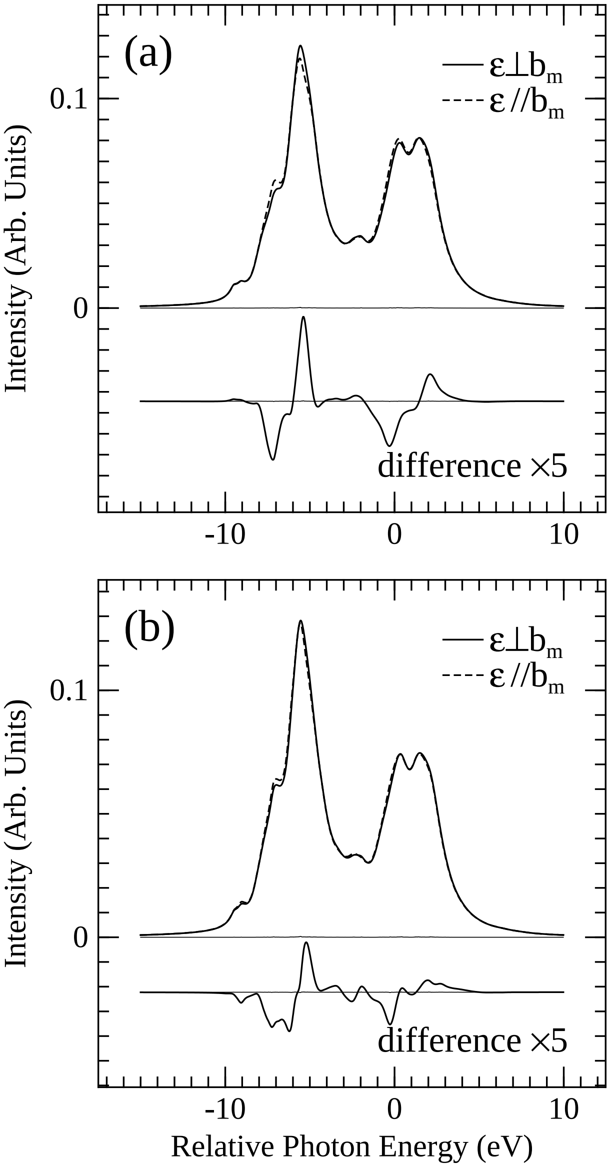

Fig. 16. Theoretical polarization-dependent V $2p$ XAS spectra for the AFI phase calculated without (a) and with (b) the $3d$ spin-orbit interaction. $D_{\rm trg} = 0.28$ eV is assumed. The spectra are depicted for two different directions of the polarization vectors $\boldsymbol{\varepsilon}$ of the light: parallel and perpendicular to the monoclinic $\boldsymbol{b}_m$ axis. The difference spectra are also shown below in each panel.

Figure 15 shows the calculated spectra obtained using the V ion pair model with the polarization vectors $\boldsymbol{\varepsilon}$ parallel and perpendicular to the $\boldsymbol{c}_h$-axis. In Fig. 15(a) the spectra for the PM phase, and in Fig. 15(b) those for the AFI phase are shown and in each panel, the difference spectrum is also depicted. The theoretical spectra well reproduce experimental ones especially those for the AFI phase in ref. 14. Although the difference spectrum for the PM phase is less similar to the experimental one, its tendency to have negative peaks at -7 eV and 0 eV is consistent with the experiment. The polarization of the spectra defined by $P = (I_{\parallel} - I_{\perp})/(I_{\parallel} + I_{\perp})$ are $P = 0.027$ for the AFI phase and $P = 0.015$ for the PM phase, where $I_{\parallel}$ and $I_{\perp}$ denote integrated intensity of the spectra with the light polarization parallel and perpendicular to the $\boldsymbol{c}_h$-axis, respectively. Such large change in the polarization between the two phases is also consistent with the experiment. Note that although the electron occupation of the e^{σ} orbitals in the ground state is small $\sim 5\%$, the inclusion of the e^{σ} orbital is important to reproduce the spectra, especially its polarization.

The sensitivity of the V $2p$ XAS spectra with polarized light to the orbital occupation in the initial state is useful to ascertain whether the orbital order exists or not in the AFI phase. To demonstrate this, in Fig. 16 the polarization-dependent V $2p$ XAS spectra are shown for two different direction of $\boldsymbol{\varepsilon}$ in the plane which is perpendicular to the $\boldsymbol{c}_h$-axis: $\boldsymbol{\varepsilon} \perp \boldsymbol{b}_m$ and $\boldsymbol{\varepsilon} // \boldsymbol{b}_m$. The spectra without (a) and with (b) the $3d$ spin-orbit interaction is presented; other parameters are the same to those adopted for the AFI phase. The difference spectra are also shown below in each panel.

As was discussed in § 2.3, in the absence of the $3d$ spin-orbit interaction, the ground state has an orbital polarization corresponding to the molecular ferro-orbital ordering state of Milla's model (Fig. 16(a)). On the other hand, in the presence of the spin-orbit interaction, the ground state has no orbital ordering and instead of this a large orbital magnetic moment is induced in the ground state (Fig. 16(b)). The magnitude of the difference spectrum in Fig. 16(a) is much larger than that in Fig. 16(b) and the shape of the spectrum in Fig. 16(a) largely vary from that in Fig. 16(b). Thus the measurement of this linear dichroic V $2p$ spectra, will be a crucial check whether the large orbital moment is present or not.

§7. Conclusions

The $3d$ electronic structure and phase transition in pure and Cr doped V_2O_3 were theoretically investigated in relation to the $3d$ spin-orbit interaction and lattice distortion. The $3d$ electronic state of V_2O_3 have been discussed, using a V ion pair model on the basis of the configuration interaction approach. In the model, the $3d$-$3d$ multipole interaction, a trigonal crystal field and the $3d$ spin-orbit interaction were considered and electron hopping between nearest neighbor V ions was also taken into account. In the presence of the $3d$ spin-orbit interaction, spin and orbital degrees of freedom are strongly coupled and this removes the orbital degeneracy of the ground state, resulting in no orbital ordering. Instead of this, each V ion with $S = 1$ spin state has a large orbital magnetic moment $\sim 0.7\mu_{\mathrm{B}}$ in the AFI phase. These results are in contrast to those obtained from the similar V ion pair model proposed by Mila *et al.*, in which a ferro molecular orbital ordering occurs in the AFI phase.[18, 19] The large orbital moment is in accordance with the ratio $M_{\mathrm{L}}/M_{\mathrm{S}} \sim -0.3$ deduced from the nonresonant magnetic x-ray scattering experiment[20] and also explains small total magnetic moment $1.2\mu_{\mathrm{B}}$ observed in the AFI phase.[8] Because of the presence of the large orbital magnetic moment, the monoclinic lattice distortion and the direction of the magnetic easy axis is strongly connected in the AFI phase. The direction of magnetic moment was found to be canted from the corundum $\boldsymbol{c}_h$-axis in the presence of the monoclinic distortion and this agrees with the neutron diffraction experiments.[8]

The local lattice distortion energy due to tilting of the V ion pair from the corundum c-axis was further considered. From the present model, it is expected that there is at least two local minima for the free energy in the real system as a function of the V-V distance of the pair. One is positioned at the V-V distance in the PM phase, where the energy difference of the two kinds of the state $e^{\pi}a_1; e^{\pi}e^{\pi}$ and $e^{\pi}e^{\pi}; e^{\pi}e^{\pi}$ is large and thus no electron-lattice coupling takes place. The electronic state of the V ion pair in this phase is described as a superposition of two configurations $e^{\pi}a_1; e^{\pi}e^{\pi}$ and $e^{\pi}e^{\pi}; e^{\pi}a_1$ in equal weight, which is similar to Mila's model. The other one is located at the V-V distance in the PI and AFI phases, where energies of the two kinds of the states are degenerate and Jahn-Teller like lattice distortion is the cause of the energy lowering at this V-V distance. Because of the tilting of the V ion pair caused by this lattice instability, the $e^{\pi}e^{\pi}; e^{\pi}e^{\pi}$ state is further hybridized with above $e^{\pi}a_1; e^{\pi}e^{\pi}$ ($e^{\pi}e^{\pi}; e^{\pi}a_1$) state in these phases. This large difference in the electron occupation between the metal and insulating phases agrees with the recent linear dichroic V $2p$ x-ray absorption spectroscopy (XAS) experimental results.[14]

Since both in the AFI and PI phases, the electron-lattice coupling strongly influences the orbital occupation and charge fluctuation, the PM → AFI and PM → PI transitions can not be regarded as usual Mott transition. The elongation of the V-V distance and resultant reduction in the hybridization strength between the $3d$ orbitals caused by this electron-lattice coupling is probably responsible for these metal-insulator transitions.

To investigate interplay between magnetic ordering and the lattice distortion, an effective spin Hamiltonian including the effects of tilting of the V ion pairs was introduced. The antiferromagnetic order with the monoclinic lattice distortion observed in the AFI phase was reproduced in this model, where simultaneous ordering of the tilting directions and the magnetic moments of the V ion pairs take place. With increasing temperature, it exhibits antiferromagnetic to paramagnetic phase transition corresponding to the AFI → PI transition in the real system. While all V ion pairs are tilted to the same direction and this gives rise the monoclinic lattice distortion in the AFI phase, their tilting directions are disordered and fluctuate among the three stable directions in the PI phase. As a result, there is no monoclinic distortion in the PI phase. It was also found that the C_{44} elastic constant softens and short-range spin correlation functions abruptly changes at this second order transition in this model. These results are consistent with the ultrasonic-wave measurement[11] and recent neutron scattering experiments.[9, 10]

To confirm the validity of the present model, recent experiments on the resonant X-ray scattering (RXS) at the V K-edge[20, 21] and the linear dichroic V $2p$ XAS experiments[14] were analyzed. The (111) Bragg reflection observed in the RXS experiments, particularly in its azimuthal angle and polarization dependence of the $1s \to 3d$ peak, is well explained within the present model, where no orbital ordering is present and the antiferromagnetic order is assumed. The reflection is pure magnetic and the scattering amplitude of this reflection mainly arises from the interference process of the $1s \to 4p$ dipole and $1s \to 3d$ quadrupole transitions. The shape and magnitude of the linear dichroic V $2p$ XAS spectra in both the AFI and PM phases are well reproduced within the present model. Another linear dichroic V $2p$ XAS experiment has been proposed, which is sensitive to the presence of the orbital order in the initial state and will be a crucial check to the present model.

This work is partly supported by a Grant-in-Aid for Scientific Research from the Ministry of Education, Culture, Sports, Science and Technology.

---

[1] N. F. Mott: *Metal Insulator Transitions* (Taylor & Francis, London, 1974).

[2] P. D. Dernier and M. Marezio: Phys. Rev. B **2** (1970) 3771.

[3] D. B. McWhan and J. P. Remeika: Phys. Rev. B **2** (1970) 3734.

[4] A. Jayaraman, D. B. McWhan, J. P. Remeika and P. D. Dernier: Phys. Rev. B **2** (1970) 3751.

[5] A. Menth and J. P. Remeika: Phys. Rev. B **2** (1970) 3756.

[6] D. B. McWhan, A. Menth, J. P. Remeika, W. F. Brinkman and T. M. Rice: Phys. Rev. B **7** (1973) 1920.

[7] H. Kuwamoto, J. M. Honig and J. Appel: Phys. Rev. B **22** (1980) 2626.

[8] R. M. Moon: Phys. Rev. Lett. **25** (1970) 527; J. Appl. Phys. **41** (1970) 883.

[9] W. Bao, C. Broholm, G. Aeppli, P. Dai, J. M. Honig and P. Metcalf: Phys. Rev. Lett. **78** (1997) 507.

[10] W. Bao, C. Broholm, G. Aeppli, S. A. Carter, P. Dai, T. F. Rosenbaum, J. M. Honig, P. Metcalf and S. F. Trevino: Phys. Rev. B **58** (1998) 12727.

[11] H. Yang, R. J. Sladek and H. R. Harrison: Solid State Commun. **47** (1983) 955.

[12] M. Yethiraj, S. A. Werner, W. B. Yelon and J. M. Honig: Phys. Rev. B **36** (1987) 8675.

[13] C. Castellani, C. R. Natoli and J. Ranninger: Phys. Rev. B **18** (1978) 4945; *ibid* B **18** (1978) 4967.

[14] J.-H. Park, L. H. Tjeng, A. Tanaka, J. W. Allen, C. T. Chen, P. Metcalf, J. M. Honig, F. M. F. de Groot and G. A. Sawatzky: Phys. Rev. B **61** (2000) 11506.

[15] V. I. Anisimov, J. Zaanen and O. K. Andersen: Phys Rev. B **44** (1991) 943.

[16] V. I. Anisimov, F. Aryasetiawan and A. I. Liechtenstein: J. Phys.: Condens. Matter **9** (1997) 767.

[17] S. Yu. Ezhov, V. I. Anisimov, D. I. Khomskii and G. A. Sawatzky: Phys. Rev. Lett. **83** (1999) 4136.

[18] F. Mila, R. Shiina, F.-C. Zhang, A. Joshi, M. Ma, V. Anisimov and T. M. Rice: Phys. Rev. Lett. **85** (2000) 1714.

[19] R. Shiina, F. Mila, F.-C. Zhang and T. M. Rice: Phys. Rev. B **63** (2001) 144422.

[20] L. Paolasini, C. Vettier, F. de Bergevin, F. Yakhou, D. Mannix, A. Stunault W. Neubeck, M. Altarelli, M. Fabrizio, P. A. Metcalf and J. M. Honig: Phys. Rev. Lett. **82** (1999) 4719.

[21] L. Paolasini, S. Di Matteo, C. Vettier, F. de Bergevin, A. Sollier, W. Neubeck, F. Yakhou, P. A. Metcalf and J. M. Honig: J. Elect. Spect. Relat. Phenom. **120** (2001) 1.

[22] J. W. Allen: Phys. Lett. **36** (1976) 1249.

[23] S. W. Lovesey and K. S. Knight: J. Phys.: Condens. Matter **12** (2000) L367.

[24] A. Tanaka and T. Jo: J. Phys. Soc. Jpn. **63** (1994) 2788.

[25] H. Eskes and G. A. Sawatzky: Phys. Rev. B **43** (1991) 119.

[26] A. Tanaka and T. Jo: J. Phys. Soc. Jpn. **65** (1996) 912.

[27] S. Sugano, Y. Tanabe and H. Kamimura: *Multiplets of Transition-Metal Ions in Crystal* (Academic Press, New York, 1970).

[28] A. E. Bocquet, T. Mizokawa, K. Morikawa, A. Fujimori, S. R. Barman, K. Maiti, D. D. Sarma, Y. Tokura and M. Onoda: Phys Rev. B **53** (1996) 1161.

[29] T. Uozumi, K. Okada, A. Kotani, R. Zimmermann, P. Steiner, S. Hüfner, Y. Tezuka and S. Shin: J. Elect. Spect. Relat. Phenom. **83** (1997) 9.

[30] T. Uozumi, K. Okada and A. Kotani: J. Elect. Spect. Relat. Phenom. **78** (1996) 103.

[31] W. A. Harrison: *Electronic Structure and Physical Properties of Solids* (Freeman, San Francisco, 1980).

[32] T. M. Rice: *Spectroscopy of Mott Insulators and Correlated Metals*, edited by A. Fujimori and Y. Tokura (Springer, Berlin, 1995).

[33] Doon Gibbs, D. R. Harshman, E. D. Isaacs, D. B. McWhan, D. Mills and C. Vettier: Phys. Rev. Lett. **61** (1988) 1241.

[34] J. P. Hannon, G. T. Trammell, M. Blume and Doon Gibbs: Phys. Rev. Lett. **61** (1988) 1245.

[35] D. B. McWhan, C. Vettier, E. D. Isaacs, G. E. Ice, D. P. Siddons, J. B. Hastings, C. Peters and O. Vogt: Phys. Rev. B **42** (1990) 6007.

[36] K. Hirota, N. Oumi, T. Matsumura, H. Nakao, Y. Wakabayashi, Y. Murakami and Y. Endoh: Phys. Rev. Lett. **84** (2000) 2706.

[37] M. Fabrizio, M. Altarelli and M. Benfatto: Phys. Rev. Lett. **80** (1998) 3400; *ibid* **81** (1998) 4030.

[38] P. Carra, B. T. Thole, M. Altarelli and X. Wang: Phys. Rev. Lett. **70** (1993) 694.

[39] A. Tanaka and T. Jo: J. Phys. Soc. Jpn. **61** (1992) 2040.

[40] R. Haydock, V. Heine and M. J. Kelly: J. Phys C **5** (1972) 2845.